ANL-7245

Argonne National Laboratory

REACTOR DEVELOPMENT PROGRAM

PROGRESS REPORT

July 1966

Printed in USA. Price $3.00 . Available from the Clearinghouse for Federal Scientific and Technical Information, National Bureau of Standards, U. S. Department of Commerce, Springfield, Virginia 22151

ANL-7245
Reactor Technology
(TID-4500)
AEC Research and
Development Report

0570

ARGONNE NATIONAL LABORATORY
9700 South Cass Avenue
Argonne, Illinois 60439

REACTOR DEVELOPMENT PROGRAM PROGRESS REPORT

July 1966

Albert V. Crewe, Laboratory Director
Stephen Lawroski, Associate Laboratory Director

Division	Director
Chemical Engineering	R. C. Vogel
Idaho	M. Novick
Metallurgy	M. V. Nevitt
Reactor Engineering	L. J. Koch
Reactor Physics	R. Avery
Remote Control	R. C. Goertz

Report coordinated by
R. M. Adams and A. Glassner

Issued August 26, 1966

Operated by The University of Chicago
under
Contract W-31-109-eng-38
with the
U. S. Atomic Energy Commission

FOREWORD

The Reactor Development Program Progress Report, issued monthly, is intended to be a means of reporting those items of significant technical progress which have occurred in both the specific reactor projects and the general engineering research and development programs. The report is organized in a way which, it is hoped, gives the clearest, most logical overall view of progress. The budget classification is followed only in broad outline, and no attempt is made to report separately on each sub-activity number. Further, since the intent is to report only items of significant progress, not all activities are reported each month. In order to issue this report as soon as possible after the end of the month editorial work must necessarily be limited. Also, since this is an informal progress report, the results and data presented should be understood to be preliminary and subject to change unless otherwise stated.

The issuance of these reports is not intended to constitute publication in any sense of the word. Final results either will be submitted for publication in regular professional journals or will be published in the form of ANL topical reports.

The last six reports issued
in this series are:

January 1966	ANL-7152
February 1966	ANL-7176
March 1966	ANL-7193
April 1966	ANL-7204
May 1966	ANL-7219
June 1966	ANL-7230

REACTOR DEVELOPMENT PROGRAM

Highlights of Project Activities for July 1966

EBR-II

A short, zero-power run was made to irradiate flux wires. Run No. 20, scheduled for 700 MWd, has been started.

The limit of Mark-IA fuel has been set temporarily at 1.2 a/o burnup on the basis of surveillance measurements.

ZPR-3

Fast-neutron-spectral measurements and fission ratios relative to U^{235} have been made with Assembly 48.

ZPPR

The construction contract was signed with Arrington Construction Co., Idaho Falls.

TABLE OF CONTENTS

TABLE OF CONTENTS

TABLE OF CONTENTS

TABLE OF CONTENTS

I. CIVILIAN POWER REACTORS

A. Plutonium Utilization

1. Capture-to-fission Ratios of Pu^{239} and Pu^{241} in EBWR

The Experimental Boiling Water Reactor (EBWR) is currently partially loaded with recycled plutonium fuel. An experiment designed to measure the capture-to-fission ratio of Pu^{239} and Pu^{241} during power operation, consists in exposing specially prepared Pu^{239} foils for different irradiation periods and analyzing the irradiation products. In the proposed experiment a specially designed mounting unit is inserted between four fuel rods on a square lattice to hold a specially designed foil assembly flush with each fuel rod.

It is necessary to first determine the effects of the mounting unit on the fuel rods. The study must cover

a. change in coolant flow and steam void concentration;

b. temperature at the interface of the Zircaloy clad and cadmium cover of the foil assembly.

a. Effect of the Mounting Unit. To evaluate the effect of the mounting unit on the fluid flow rate, the following assumptions were made:

(i) The effect of the mounting is local, being confined to the boiling zone.

(ii) This effect consists of a redistribution of components of pressure drops, their sum remaining unchanged.

(iii) The effect of the mounting is to reduce the flow rate v, and increase the steam void fraction, keeping their product nearly constant.

The results of calculations indicate that the flow velocity will be reduced by about 20% (and steam void increased by approximately 20%) due to insertion of the mounting unit.

b. Temperature at the Fuel Rod and Foil Interface. Hot spots could result if there were large contact resistances in the gap between the components of test units (foil assemblies). The material cross section of the test (foil) assembly (see Fig. 1) consists of:

0.005-in. circular clad + a possible helium gap of 0.00312 in. + 0.020 in. of cadmium + 0.005-in. Al-Pu capsule + 0.005 in. of Zircaloy clad.

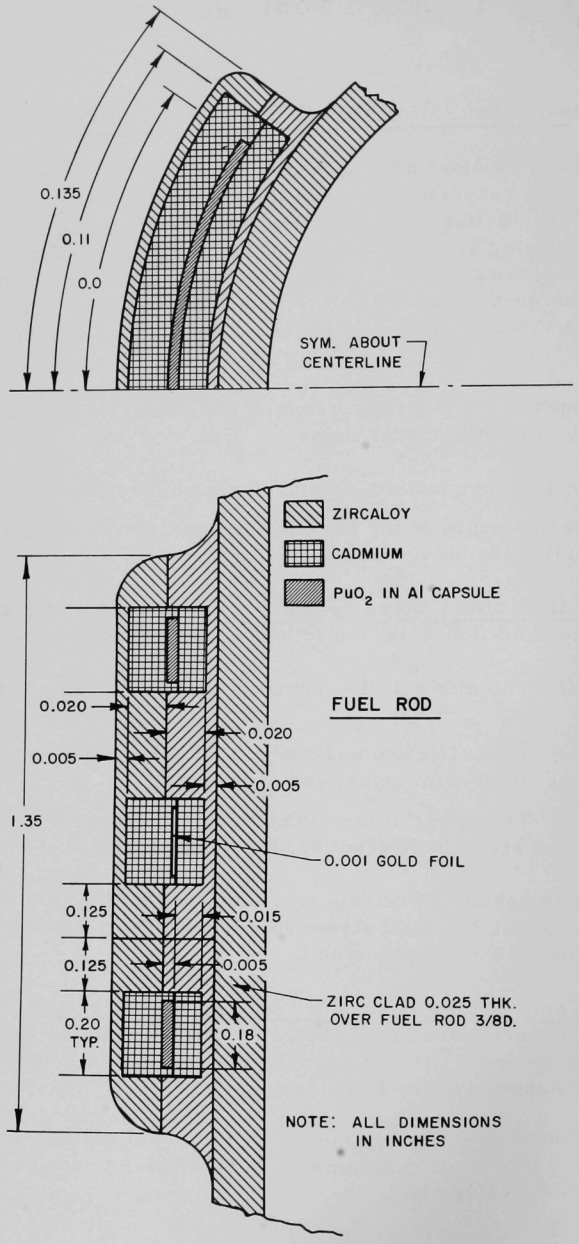

Fig. 1. Sectional View of the Foil Assembly Used in Measurement of the Capture-to-fission Ratios of Pu^{239} and Pu^{241} with the EBWR in Ope...

If a 0.00312-in. helium gap surrounded the fuel element, there could be a temperature rise ΔT_{gap} of ~200°F. Actually, the temperature rise should be much smaller, due to dissipation of heat in three dimensions.

To allow for dissipation of heat, three-dimensional calculations were made by the THTB code.[1] The maximum temperatures in the Zircaloy clad and in the cadmium obtained from the above calculations are given in Table I for various conditions of flow. In all cases the centerline temperature of the fuel rod was taken as ≲920°F.

TABLE I. A Resume of Results of THTB Code Calculations

(Temperatures are in °F)

For all cases $T_{centerline\ of\ fuel\ rod} \approx 920°F$.

	T_{clad}	$T_{cadmium}$
I. Full flow rate around fuel rods		
1) Zero contact resistance	552	514
2) Contact resistance* over 1/3 area, cadmium to Zircaloy	565	537
3) Contact resistance over all of area, cadmium to Zircaloy	600	575
II. 50% of full flow around half of rod, covering test specimen (Full flow over remaining area)		
1) Zero contact resistance	560	521
2) Contact resistance over 1/3 area, cadmium to Zircaloy	574	544
3) Contact resistance over all of area, cadmium to Zircaloy	607	581
III. 25% of full flow around half of rod, covering test specimen (Full flow over remainder)		
1) Zero contact resistance	571	533
2) Contact resistance over 1/3 area, cadmium to Zircaloy	583	555
3) Contact resistance over all of area, cadmium to Zircaloy	616	592
IV. 1% of full flow around test specimen (Full flow over remainder of rod area)		
1) Zero contact resistance	625	602
2) Contact resistance over all of area, cadmium to Zircaloy	646	629

*Contact resistance due to helium gap of 0.00312 in.

It should be stated that the helium gap of 0.00312 in. is conservative, since a radiographic profile of the test samples should detect a gap of 0.002-0.003 in.

[1]Stephens, G. L., and Campbell, D. J., Program THTB for Analysis of General Transient Heat Transfer Systems, GE Report R-60FPD 647 (April 1961).

It is seen from the data of Table I that, even if the fluid flow rates around the test specimen were reduced by 99% and a helium gap of 0.00312 in. existed, with $T_{centerline\ of\ fuel}$ is ≈920°F, T_{clad} is 629°F. The latter temperature is well below the 750°F tentatively set as a limit to prevent undue thermal stress in the clad.

It is also seen from Table I that, even if the flow rates were reduced by 75% and the helium gap existed, $T_{cadmium} = 592°F$.

Finally, it is pointed out that the anticipated flow reduction should be only 20% (not 75%), and gaps of ≲0.003 in. can be detected. Hence, it is not anticipated that any meltdown of cadmium nor damage of Zircaloy clad should occur.

c. Preparation of Miniature Plutonium Samples. The preparation of samples of Pu^{239} and Pu^{241} for capture-to-fission measurements in EBWR can be separated into four operations:

(i) deposition of the sample on the aluminum;

(ii) determination of the mass of the sample;

(iii) sealing by cold welding;

(iv) leak testing.

Because of the restrictions on the physical dimensions, i.e., the requirement of miniature samples, the first two operations become very difficult. The remaining two operations are not affected by sample size and have already been suitably developed.

A technique has been developed in which plutonium samples can be confined to a diameter of 0.125 in. In this method, aluminum discs, 0.003 in. thick and 0.750 in. in diameter, are prepared with a small depression in the center (0.125 in. in diameter and about 0.003 in. deep). A drop of plutonium-bearing solution, about 2λ in volume, is deposited in the depression. Although there is some tendency for the drop to spread out, it remains within the confines of the depression. Acceptable deposits and fairly uniform samples have been made with 250-300 μg of plutonium in a circular area of 0.125-in. dia.

The masses of such samples are usually determined by accurately pipetting a known volume of solution whose concentration has been established directly or indirectly by some gravimetric method. In this case, since 2λ volumes are being pipetted, it is doubtful whether the mass could be determined to within 25% by such small volume measurements. In addition, to make the measurements gravimetrically it would be necessary to have a microbalance inside of the glove hood where the samples are prepared, and these facilities are not presently available.

A more accurate method which has been successfully employed is to alpha count the samples. The activity can easily be counted in a low-geometry chamber which is already available. The thickness of these samples will be about 3 mg/cm^2, so there should be no self-absorption losses. The solid angle[2] can be calculated to within an uncertainty of about 0.1%, so that the error in the activity should be of the order of the errors in the half-lives involved. After the samples have been pipetted and dried on the aluminum planchets, they are counted in the low-geometry chamber. The mass of each sample can be determined from the measured absolute activity and the calculated specific activity.

B. Liquid-metal Fast Breeder Reactors

1. Fuel Development

a. Metal Fuels

(i) Irradiation of Uranium-Plutonium Alloys. Twenty full-length (14 in.) metal fuel rods are undergoing irradiation in the EBR-II reactor. Eighteen have U-Pu-Zr alloy pins jacketed in either V-20 w/o Ti, Type 304 stainless steel, Type 316 stainless steel, Hastelloy-X, or Hastelloy-X-280 tubing. These rods are operating at maximum jacket temperatures of 630°C and at present have reached a calculated maximum 3.5 a/o burnup. Two additional rods, fueled with U-Pu-Ti alloy and jacketed in V-20 w/o Ti alloy tubing, are being irradiated at maximum jacket temperatures of 540°C and have attained a maximum burnup of 3.4 a/o. Additional details on the design of the fuel rods and the irradiation conditions are summarized in Table II.

Five instrumented, temperature-controlled capsules, now being operated in the CP-5 reactor, contain several different types of experimental alloy fuels. Table II also summarizes information on these specimens.

U-Pu-Zr alloy is being irradiated in CP-5 in V-20 w/o Ti alloy tubing and has reached a calculated 9.3 a/o burnup at a maximum jacket temperature of 630°C. This capsule has been neutron radiographed and the specimen is in good condition. A measurement of the height of the fuel column shows that there has been no change since the last radiograph taken at 4.2 a/o burnup.

A U-Pu-Ti alloy specimen also jacketed in V-20 w/o Ti alloy tubing has attained a calculated 8.1 a/o burnup at maximum jacket temperatures of 560°C. This fuel rod was also recently neutron radiographed and the specimen was noted to be in good condition. A previous

---

[2]Jaffey, A. H., Solid Angle Subtended by a Circular Aperture at Point and Spread Sources, Rev. Sci. Instr. 25, 349-354 (1954).

neutron radiograph taken at 4.6 a/o burnup showed a fuel elongation of 15%. No additional change in length was noted in radiograph.

TABLE II. Status of Metal Fuel Irradiations in Progress

			Design Parameters					Operating Conditions			
										Burnup to Date	
Test Reactor	Capsule or S/A No.	Specimen Number	Fuel Composition (w/o)	Effective Density (%)	Cladding Composition (w/o)	Cladding OD (in.)	Cladding Thickness (in.)	kW/cc[a]	Max Cladding Temp (°C)	a/o (U + Pu)	fiss/cc x 10^{-20}[a]
CP-5	CP-45	1N15	U-19 Pu-14 Zr	66	V-20 Ti	0.208	0.015	2.6	630	9.3	20.2
EBR-II	XG06	ND23	U-15 Pu-10 Zr	66	V-20 Ti	0.209	0.016	1.7	540	3.4	8.1
EBR-II	XG05	ND24	U-15 Pu-10 Zr	66	V-20 Ti	0.209	0.016	1.7	535	3.1	7.4
EBR-II	XA07	ND28	U-15 Pu-9 Zr	75	304 SS	0.208	0.021	2.0	630	3.5	9.8
EBR-II	XA07	ND41	U-15 Pu-9 Zr	75	304 SS	0.208	0.021	2.0	625	3.4	9.5
EBR-II	XA07	ND32	U-15 Pu-9 Zr	75	316 SS	0.196	0.015	2.0	605	3.2	8.9
EBR-II	XA07	ND43	U-15 Pu-9 Zr	75	Hastelloy-X	0.196	0.015	2.0	615	3.3	9.2
EBR-II	XA07	ND25	U-14 Pu-12 Zr	76	304 SS	0.208	0.021	1.9	600	3.0	7.8
EBR-II	XA07	ND27	U-14 Pu-12 Zr	76	304 SS	0.208	0.021	1.9	605	3.1	8.0
EBR-II	XA07	ND26	U-14 Pu-12 Zr	76	316 SS	0.196	0.015	1.8	590	2.9	7.5
EBR-II	XA07	ND29	U-14 Pu-12 Zr	76	316 SS	0.196	0.015	1.8	595	3.0	7.8
EBR-II	XA07	ND30	U-14 Pu-12 Zr	76	316 SS	0.196	0.015	1.9	615	3.3	8.5
EBR-II	XA07	ND31	U-14 Pu-12 Zr	76	316 SS	0.196	0.015	1.9	610	3.2	8.3
EBR-II	XA07	ND33	U-14 Pu-12 Zr	76	Hastelloy-X	0.196	0.015	1.9	605	3.2	8.3
EBR-II	XA07	ND34	U-14 Pu-12 Zr	76	Hastelloy-X	0.196	0.015	1.9	610	3.2	8.3
EBR-II	XA07	ND35	U-14 Pu-12 Zr	76	Hastelloy-X	0.196	0.015	1.9	615	3.3	8.1
EBR-II	XA07	ND37	U-14 Pu-12 Zr	66	Hastelloy-X-280	0.208	0.015	1.8	610	3.3	8.2
EBR-II	XA07	ND39	U-14 Pu-12 Zr	66	Hastelloy-X-280	0.208	0.015	1.8	610	3.3	8.2
EBR-II	XA07	ND44	U-14 Pu-12 Zr	66	Hastelloy-X-280	0.208	0.015	1.8	600	3.2	8.0
CP-5	CP-44	1N14	U-15 Pu-10 Ti	69	V-20 Ti	0.203	0.015	2.4	560	8.1	18.6
EBR-II	XG05	NC17	U-15 Pu-10 Ti	63	V-20 Ti	0.209	0.016	1.6	540	3.2	7.0
EBR-II	XG06	NC23	U-15 Pu-10 Ti	63	V-20 Ti	0.209	0.016	1.6	540	3.4	7.5
CP-5	CP-41	4N10	U-10 Pu-10 Fz	77	V-20 Ti	0.196	0.016	1.9	530	7.5	22.1
CP-5	CP-41	5N11	U-10 Pu-10 Fz	79	V-20 Ti	0.193	0.016	2.0	530	7.5	22.5
CP-5	CP-41	6N12	U-10 Pu-10 Fz	84	V-20 Ti	0.189	0.016	2.1	530	7.5	24.0
CP-5	CP-41	1N7	U-15 Pu-10 Fz	77	V-20 Ti	0.196	0.016	1.9	530	7.5	22.1
CP-5	CP-41	2N8	U-15 Pu-10 Fz	79	V-20 Ti	0.193	0.016	2.0	530	7.5	22.5
CP-5	CP-41	3N9	U-15 Pu-10 Fz	84	V-20 Ti	0.189	0.016	2.1	530	7.5	24.0
CP-5	CP-43	1N13	U-15 Pu-10 Fz	73	V-20 Ti	0.199	0.015	2.3	540	7.1	19.8
CP-5	CP-50	1N16	Th-20 U	75	V-20 Ti	0.196	0.015	1.9	600	4.8	2.2
CP-5	CP-50	4N19	Th-20 U	75	V-20 Ti	0.196	0.015	1.9	600	4.8	2.2
CP-5	CP-50	2N17	Th-10 Pu-10 U	75	V-20 Ti	0.196	0.015	2.0	630	5.5	2.5
CP-5	CP-50	5N20	Th-10 Pu-10 U	75	V-20 Ti	0.196	0.015	2.0	630	5.5	2.5
CP-5	CP-50	3N18	Th-10 Pu-20 U	75	V-20 Ti	0.196	0.015	1.9	630	3.2	2.3
CP-5	CP-50	6N21	Th-10 Pu-20 U	75	V-20 Ti	0.196	0.015	1.9	600	3.2	2.3

[a]Based on effective density.

The cessation of lengthwise growth in these two specimens is not unusual, as similar behavior has been observed in other metal irradiation specimens wherein release of the fission gases in the fuel had occurred.

A metallographic examination is being conducted of U-15 w/o Pu-10 w/o Fz and U-10 w/o Pu-10 w/o Fz alloy fuel pins jacketed in Nb-1 w/o Zr tubing having wall thicknesses between 0.015 and 0.025 in. These specimens had been irradiated to a maximum of 8.7 a/o burnup and an average jacket temperature of 430°C. The effective fuel density of the specimens was 85.2%. The average change of fuel volume at the end of the irradiation was found to be 24%.

The preliminary macroscopic examination of transverse as well as longitudinal sections of the specimens shows that there had been no reaction between fuel and the jacketing. The fuel material is characterized by pores approximately 4 μ in diameter near the outer edge. The

pores in the center of the rod were approximately 15 μ in diameter. The data on fission-gas recovery indicate that the fuel specimens released from 3.7 to 9.6% of the theoretical yield.

Capsule CP-50 containing six Th-U and Th-U-Pu fuel alloys, jacketed in V-20 w/o Ti tubing, is also being irradiated in the CP-5 reactor. The objectives of the experiment are to determine the relative swelling behavior of the fuels, the restraint characteristics of the jacket, and the maximum attainable burnup before jacket failure.

U-Pu-Fz alloy specimens being irradiated in CP-5 are designed for a study of fuel-density parameters having a direct bearing on maximum attainable burnup. These specimens have reached a maximum burnup of 7.5 a/o at maximum cladding temperatures of 530°C.

b. Ceramic Fuels

(i) Irradiations in EBR-II. The status of experimental fuel rods of mixed oxide and mixed carbide is shown in Tables III and IV. Four new rods containing physically mixed UC and PuC powders, virbrationally compacted solid solution (U,Pu)C powder, and UC-20 w/o PuC pellets, were loaded into capsules and sodium bonded preparatory to irradiation in EBR-II.

TABLE III. Status of UC-20 w/o PuC Fuel Irradiations in EBR-II

		Design Parameters				Operating Conditions			
								Burnup to Date	
Capsule or S/A No.	Specimen Number	Effective Density (%)	Cladding Composition (w/o)	Cladding OD (in.)	Cladding Thickness (in.)	kW/cc[a]	Max Cladding Temp (°C)	a/o (U + Pu)	fiss/cc x 10^{-20}[a]
XG05	SMV-2	84	304 SS	0.297	0.020	2.1	645	3.1	8.6
XG05	HMV-5	80	Hastelloy-X	0.297	0.015	2.2	670	3.2	8.5
XG05	NMV-11	84	Nb-1 w/o Zr	0.281	0.012	2.1	645	3.2	9.0
XO08	NMP-2	82	Nb-1 w/o Zr	0.281	0.012	1.6	545	1.8	5.0
XO08	NMV-4	80	Nb-1 w/o Zr	0.281	0.012	2.4	635	2.6	7.0
XO08	NMV-7	80	Nb-1 w/o Zr	0.281	0.012	2.1	605	2.4	6.4
XO08	NMV-12	86	Nb-1 w/o Zr	0.281	0.012	2.4	635	2.6	7.4
XO08	HMV-1	80	Hastelloy-X	0.297	0.015	2.1	640	2.4	6.2
XO08	HMV-4	80	Hastelloy-X	0.297	0.015	2.3	670	2.6	6.8
XO08	HWMP-1	82	Hastelloy-X + W	0.297	0.020	1.6	555	1.8	4.8
XO08	HWMV-1	83	Hastelloy-X + W	0.297	0.020	2.4	685	2.6	7.2
XO09	SMV-1	82	316 SS	0.306	0.024	1.6	570	1.9	5.1
XO09	SMP-1	80	316 SS	0.306	0.024	2.1	640	1.5	3.9
XO09	VMV-1	86	Vanadium	0.301	0.022	2.5	640	2.2	6.2

[a]Based on effective density.

TABLE IV. Status of UO_2-20 w/o PuO_2 Fuel Irradiations in EBR-II

		Design Parameters				Operating Conditions			
								Burnup to Date	
Capsule or S/A No.	Specimen Number	Effective Density (%)	Cladding Composition (w/o)	Cladding OD (in.)	Cladding Thickness (in.)	kW/cc[a]	Max Cladding Temp (°C)	a/o (U + Pu)	fiss/cc x 10^{-20}[a]
XO09	SOV-5	82	304 SS	0.297	0.020	1.7	555	1.9	3.9
XO09	SOV-6	82	304 SS	0.297	0.020	1.7	565	2.0	4.2
XO11	SOV-3	83	304 SS	0.296	0.019	1.9	610	1.3	2.8
XO11	HOV-4	80	Hastelloy-X	0.295	0.014	1.8	600	1.3	2.6
XO11	TVOV-1	77	V-20 w/o Ti	0.297	0.020	1.7	575	1.3	2.5
XO11	SOV-7	85	304 SS	0.296	0.019	2.0	630	1.3	2.7
XO11	SOV-1	80	304 SS	0.296	0.019	1.7	590	1.3	2.6
XO11	HOV-10	86	Hastelloy-X	0.295	0.014	1.9	615	1.3	2.7
XO11	HOV-15	80	Hastelloy-X	0.295	0.014	1.7	590	1.3	2.5

[a]Based on effective density.

(ii) Oxide-Cermet Irradiations in EBR-II. Stainless steel-PuO_2 cermet specimens under irradiation in EBR-II are summarized in Table V. These specimens were manufactured by Battelle Northwest Laboratories and prepared for irradiation by Argonne National Laboratory.

TABLE V. Status of Cermet Fuel Irradiations in EBR-II

Capsule or S/A No.	Specimen Number	Design Parameters: Fuel Composition (w/o)	Effective Density (%)	Cladding Composition	Cladding OD (in.)	Cladding Thickness (in.)	Operating Conditions: kW/cc[a]	Max Cladding Temp (°C)	Burnup to Date: a/o (U + Pu)	Burnup to Date: fiss/cc x 10^{-20}[a]
X011	5P-9	SS-40 PuO_2	98	304 SS	0.301	0.015	0.88	495	1.8	1.4
X011	5P-12	SS-27 PuO_2	99	304 SS	0.294	0.015	0.59	450	1.8	0.89
X011	5U-14	SS-27 UO_2	98	304 SS	0.298	0.013	0.45	435	1.4	0.71

[a]Based on effective density.

(iii) Mixed-oxide Irradiations in Enrico Fermi Reactor. A proposal for the irradiation of UO_2-20 w/o PuO_2 ceramic rods in the Fermi reactor was assembled for review by Atomic Power Development Associates, Inc. The fuel rods are to be made up of vibratorily compacted microspheres manufactured by the sol-gel process at Oak Ridge National Laboratory. A rod design incorporating fission-product-gas storage areas below as well as above the fuel is to be evaluated. The rods are to be irradiated without encapsulation in the primary coolant.

(iv) Preparation of Ceramic Fuels for Fast Reactors. Uranium and plutonium carbides are being prepared by a fluidized-bed technique in which uranium or uranium-plutonium alloy is hydrided and then carbided by reaction with a methane-hydrogen fluidizing gas (see Progress Reports for February and June 1966, ANL-7176, p. 67, and ANL-7230, p. 45).

(α) Uranium Monocarbide. Because of the complications in operating experimental equipment with plutonium, equipment design and operational concepts are being tested in preparations of uranium monocarbide. The UC experiments are being carried out in a closed reactor system mounted in an open hood, whereas the (U,Pu)C experiments (described below) are being conducted in a glovebox.

A semiworks-scale fluidized-bed reactor with an internal diameter of $2\frac{1}{2}$ in. was installed and is now being used for the preparation of UC on a 2-kg scale. (Previously, UC was prepared on a 200-g scale in a $1\frac{1}{2}$-in.-dia reactor, which was designated as "Small-scale Reactor" in Progress Report for February 1966, ANL-7176, pp. 70-71.) The new reactor, which is capable of operation at pressures up to 10 atm and temperatures up to 900°C, is constructed of Type 304 stainless steel. It has a jacketed heating section which is pressurized with argon to balance the internal pressure and thus minimize the stress on the heated wall. The reactor was designed to be operated in an air environment and to discharge the product by conveying it pneumatically through a discharge tube to a product receiver that can be removed and opened in a helium-atmosphere glovebox.

Run conditions and results of the shakedown runs with $2\frac{1}{2}$-in.-dia reactor are given in Table VI. Uranium rods, 3/8 in. in diameter by 1 in. long, were charged to the reactor through a charging lock. After hydriding the uranium to completion, as indicated by unchanging hydrogen pressure, the powdered UH_3 was carbided at 15 psig. (This modest pressure was used to conserve hydrogen, since equipment for recirculation of the off-gas had not yet been installed.) The methane concentration was such that UC was the equilibrium solid phase and the higher carbides would be expected to be unstable. The methane concentrations in the inlet and outlet streams were determined by infrared analyses.

TABLE VI. Uranium Carbide Synthesis in Semiworks Reactor

	UC-6S	UC-7S	UC-8S	UC-9S
Charge (g)	1000	1700	2000	2000
Hydriding cycles	1	1	1	3
Inlet methane conc (v/o)	5.0	6.2	5.0	5.0
Carbiding time (min)	340	565	511	460
Carbiding temperature (°C)	750	750	800	800
Carbiding pressure (psig)	15	15	15	15
Total product transferred (g)	1035	1804	1922	1700
Product analysis (w/o)				
Carbon[a]	4.0	4.8	4.2	4.6
Oxygen[b]	0.40	0.48	0.50	0.50

[a]Stoichiometric UC contains 4.8 w/o carbon.

[b]The high oxygen contents, which are not typical for this process, are due to impurities in the gas and, probably, to reaction with the glovebox atmosphere subsequent to product removal from the reactor.

The mean particle size obtained in these runs was usually about 15 to 20 μ. In the case of Run UC-9S, however, the uranium was hydrided and dehydrided three times by cycling the temperature, with the result that 97 w/o of the product was finer than 20 μ. Methane utilization was usually about 50% near the beginning of a run and tapered off to 10 to 20% after 2 or 3 hr. The fine particle size in Run UC-9S, however, resulted in a methane utilization of nearly 100% for the first $1\frac{1}{2}$ hr of carburization, that is, the methane concentration of the off-gas stream was zero, within the accuracy of the infrared analyzer.

In general, the operation of the reactor was satisfactory. However, some difficulty was encountered in fluidization and in the pneumatic discharge of the product. These difficulties are attributed to the fineness of the powder resulting from the hydriding of uranium alone. Since hydriding uranium-plutonium alloy results in larger particles, it is

believed that these difficulties will be alleviated when the $2\frac{1}{2}$-in.-dia reactor is used for the preparation of (U,Pu)C. This belief is supported by observations made during the preparation of (U,Pu)C in the small-scale, $1\frac{1}{2}$-in.-dia reactor (see below).

Since the primary purpose of the runs in the $2\frac{1}{2}$-in.-dia reactor was to test the equipment, no special efforts were made to insure products of high purity. (In previous work, described in ANL-7176, p. 70, using the small-scale reactor, stoichiometric UC with an oxygen content as low as 0.08 w/o was prepared.) The main sources of impurities in the recent runs were (1) the reagent gases and (2) the glovebox atmosphere to which the products were exposed after removal from the reactor. Work is being initiated to determine the rate of oxidation of these fine UC powders in the helium glovebox atmosphere. Means of protecting the powders from oxidation by adding a pellet binder is also being investigated; this would also inhibit oxidation prior to pressing. The binder could possibly be added before the product is removed from the fluidized bed, and thus greatly reduce the oxidation problem.

The reactor system has recently been modified to recirculate the off-gas from the fluidized-bed reactor and thereby reduce the amount of hydrogen and methane required. This is expected to reduce the impurity level in the gas stream and consequently reduce contamination of the product. After testing of the recirculation system, runs will be initiated at pressures up to 10 atm.

(β) Uranium-Plutonium Carbide. Some additional data have been obtained on the initial fluidized-bed preparation of (U,Pu)C (see Progress Report for June 1966, ANL-7230, p. 45). Six preparations of (U, 15 w/o Pu)C were carried out in the small-scale ($1\frac{1}{2}$-in.-dia) reactor under the following conditions: once-through gas flow; gas concentration, 10 v/o CH_4-90 v/o H_2; total pressure, 4 atm; bed temperature, 550 to 780°C. Except for the initial run in which carburization was incomplete, the carbon content of the products ranged from about 4.8 to 5.0 (stoichiometric (U,Pu)C contains 4.8 w/o carbon). The oxygen content was generally near 500 ppm. The mean particle size of the (U,Pu)C product, about 65-75 μ, is approximately four or five times larger than that of the UC products typically prepared by this method. No fluidization problems were encountered and the products were readily dumped from the reactor by inverting it. The nature of the products and the ease with which they were removed from the reactor suggest that the pneumatic discharge of the (U,Pu)C product from the $2\frac{1}{2}$-in.-dia reactor should not pose a problem. The (U,Pu)C experiments will be described in detail when the data are complete.

2. Fuel Cladding and Structure

a. Refractory-metal Alloys for Service in Oxygen-contaminated Sodium. The 650°C, 6.1-m/sec, cold-trapped (oxygen ~10 to 12 ppm by weight) test of V-20 w/o Ti (TV-20) (see Progress Report for June 1966, ANL-7230, pp. 26-27) has been interrupted after 116 days of exposure. V-15 w/o Ti-7.5 w/o Cr samples, started later, have been tested 89 days. Total weight gains (dissolved oxygen, no external coating) are 0.81 mg/cm^2 for TV-20 and 0.54 mg/cm^2 for V-15 w/o Ti-7.5 w/o Cr.

Additional oxygen will be added to the loop (as Na_2O_2) and equilibrated with the cold trap prior to starting a new experiment. The objective is to reproduce the initial results (weight gain versus time data) of the first run as an additional means of confirming oxygen concentration data.

V-5 w/o Cr binary alloy will also be exposed to the flowing sodium in the resumed test.

As described in ANL-7230, levitation-melted castings of the V-Cr-Al ternary type are being exposed to refreshed static sodium with about 15 ppm oxygen. The results are shown in Table VII. The V-20 w/o Cr-15 w/o Al alloy is continuing to show improved resistance as compared with TV-20.

TABLE VII. Experimental Castings Exposed to Sodium at 650°C

Alloy (Composition in w/o)	Weight Loss, mg/cm^2, after	
	7.0 days	21.0 days
V-25 Cr-10 Al	1.29	3.61
V-20 Cr-10 Al	2.40	4.30
V-20 Cr-15 Al	0.46	1.09
V-20 Ti (Annealed sheet)	9.70	22.3

3. Fuel Reprocessing

a. Skull Reclamation Process. The skull reclamation process is being developed in order to recover and purify the uranium-bearing residue or skull that is left in the crucible following the melt refining of enriched uranium alloy fuel pins discharged from the EBR-II reactor. The uranium in the skull amounts to 5 to 10% of the original charge. Although the skull reclamation process for EBR-II fuel does not recover plutonium, much of the chemistry and technology being accumulated in the course of this process development has potential utility for the processing of plutonium-uranium

oxide and carbide fuels. The skull reclamation process is being tested with nonirradiated uranium in remotely operated plant-scale equipment (~4 kg uranium per batch) comprising a reduction furnace and a retorting furnace. This program is nearly completed.

Recent work has continued the demonstration of the final step in the skull reclamation process. This step consists of retorting or solvent evaporation to recover the product uranium from a Zn-12 w/o Mg-12 w/o U ingot cast from product solution that has been transferred out of the reduction furnace. The retorting procedure consists of distilling zinc and magnesium from the Zn-Mg-U product solution under vacuum (~10 Torr) at 650 to 750°C, after which the uranium is melted (~1200°C) to form a button. A large-size (8-in. OD by 17 in. high) beryllia crucible is used in the retorting step. Nine additional plant-scale retorting runs (PSR-39 through PSR-47) were completed using Zn-Mg-U ingots from previous pilot-scale and plant-scale reduction furnace runs. The runs were conducted in two BeO crucibles furnished by the Brush Beryllium Company (see Progress Report for April 1966, ANL-7204, p. 25). One of the crucibles was used in three of the runs; this crucible had also been used in two earlier runs. The other crucible, previously unused, was used in the other six runs.

Satisfactory results were achieved in all the experiments. After the runs, the crucibles were found to be in good condition. Operation of the equipment was excellent. Uranium recoveries were considered to be satisfactory. The problem of seepage of small amounts of the liquid metal solution through the crucibles was again encountered (see Progress Report for May 1966, ANL-7219, pp. 20-21). This problem, however, is not serious, and should be overcome by improved crucible fabrication, which the Brush Beryllium Company is actively investigating. In two runs, small amounts (about 2%) of the button adhered to the crucible wall when the button was dumped. In the remaining runs, the buttons were readily and completely dumped from the crucible. Of the total zinc-magnesium distilled in these runs, only about 0.4% was unaccounted for.

Following this series of retorting runs, the argon atmosphere in the large enclosure in which the skull reclamation equipment was operated was replaced with air in order to permit access to the equipment for the purpose of examination.

b. Processes for Fast Reactor Fuels. Pyrochemical processes are being developed for fast reactor fuels of the ceramic type (e.g., oxide or carbide). A process which utilizes liquid metal-molten salt extractions and salt transport separations[3] is currently being investigated for the

[3]In the salt transport separations, the fissile and/or fertile materials are selectively transferred from one liquid metal solution (donor) to another (acceptor) by cycling a molten salt phase which acts as a carrier between the two metal solutions. Noble and refractory metal fission products remain in the donor alloy.

separation of fissile and fertile constituents of the fuel and the fission products. A conceptual process flowsheet has been described previously (see Progress Report for May 1966, ANL-7219, pp. 21-22).

(i) Oxide Reduction-Partition Step. Laboratory work is in progress which is directed toward an understanding of the mechanism of the oxide reduction-partition step of the conceptual process (see ANL-7219, p. 21). Currently, the chemical interactions of UO_2, U_3O_8, and PuO_2 with various molten salts are being studied. In recent laboratory work, the uranium concentrations in various molten salts after contact with UO_2 at 800°C have been measured with the following results:

Salt	Uranium Concentration (w/o)	
	Chloride Salt Only	With 5 m/o MgF_2 Added
$MgCl_2$	0.029	0.015
50 m/o $MgCl_2$-30 m/o NaCl-20 m/o KCl	0.023	0.015
50 m/o $MgCl_2$-50 m/o $CaCl_2$	-	0.014
59 m/o LiCl-41 m/o KCl	0.005	0.003

(ii) Salt Transport Separations

(α) Plutonium Recovery. In the recovery of plutonium which has been bred in the uranium blanket of a fast breeder reactor, a relatively small amount of plutonium must be separated from a large amount of uranium. A laboratory-scale salt transport experiment (Pu-T-5) using the crucible-in-a-crucible technique (see ANL-7219, p. 23) was completed in which plutonium was separated from a U-3 w/o Pu alloy, employed to simulate the blanket in a fast breeder reactor. A magnesium-cadmium alloy was used as the donor solvent, and 50 m/o $MgCl_2$-30 m/o NaCl-20 m/o KCl was used as the salt carrier between the donor alloy and the acceptor alloy. A high zinc-low magnesium alloy was employed as the acceptor solvent. The plutonium (in 300 g of U-3 w/o Pu) was transported at 700°C from a liquid Mg-20 w/o Cd donor alloy through the molten ternary salt to a liquid Zn-6 w/o Mg acceptor alloy. At the end of the experiment, analytical results indicated that about 89% of the plutonium had been transferred through the salt to the acceptor alloy. The analytical data showed further that the rate of plutonium transfer was still significant when the experiment was terminated. The plutonium-to-uranium ratio in the feed alloy was 0.029, whereas in the acceptor alloy the ratio was 15.5. Extrapolation of the experimental data indicates that the plutonium-to-uranium ratio would be about 11.5 when the plutonium transfer reaches the theoretical limit of 98.5% in this system.

(β) Engineering Investigations. Engineering investigations of the salt transport separations step were also continued (see Progress Report for June 1966, ANL-7230, p. 30). An additional salt transport experiment (USTP-5) was completed in which the partitioning of uranium from various refractory and noble metal fission product elements was investigated. For this experiment, the feed was prepared by dissolving uranium metal (2 kg) in molten copper-magnesium alloy (donor solvent). Representative fission products (zirconium, palladium, and niobium) were added to the alloy. In the salt transport step, which was carried out at 845°C, the uranium in the molten Cu-5 w/o Mg donor alloy was transferred incrementally to a molten Mg-35 w/o Zn acceptor alloy by cycling liquid $MgCl_2$ between the two alloys. This was accomplished by having the molten metal alloys in adjacent vessels and alternately pressuring a charge of $MgCl_2$ through a transfer line from one vessel to the other. Prior to each transfer, the salt and metal phases were mixed for 4 to 5 min to promote chemical equilibration, and then the phases were allowed to separate by settling. Analytical results showed that 99% of the uranium had been transported to the magnesium-zinc acceptor alloy in 27 cycles.[4] The precipitated uranium product was then washed with Mg-30 w/o Zn alloy, after which the wash solution was removed. The washed uranium product was dissolved in a Zn-13 w/o Mg solution which was then retorted to recover the uranium. Analyses of the uranium-zinc-magnesium product solution showed the following overall removals of fission product elements: zinconium, 99.7%; palladium, 99.99%; niobium, >99.999%.

No additional uranium transport separation experiments of this type are planned at this time, since the engineering feasibility of this separations method, which was the principal objective of these experiments, has been demonstrated.

4. Physics Development

a. ZPR-3. The experimental program with Assembly 48, a large plutonium-fueled soft spectrum critical experiment (see Progress Report for June 1966, ANL-7230, pp. 5-6), continued.

Control rod worths, the worth of edge fuel material, and control rod calibrations were completed.

In-core fast-neutron-spectrum measurements were made by a group from GE-Vallecitos Atomic Power Laboratory, who used the proton-recoil method developed by E. F. Bennett of ANL. A comparison of the results obtained from this experiment and earlier results obtained by Bennett should permit a judgement of the value of this technique for plutonium assemblies and indicate the equipment specifications necessary for future ZPR work.

[4] In these experiments the rate of uranium transport was limited by the small volumes of the tungsten crucibles used. If 100-liter vessels were used, 10 kg of uranium could be transported in less than 10 cycles, which would require a period of about 4 hr.

Because of the spontaneous fission source in the plutonium, the multiplication at which such measurements can be made is limited by the acceptable gross count rate of the electronic system. In view of this fact, 99 core drawers were removed from the reactor in an attempt to provide a low-enough count rate to permit a neutron-spectrum measurement by GE of the central core. With these drawers removed and with all 10 safety-control rods withdrawn, the neutron count rate was still too high for processing by the GE equipment, although it was the same count rate that Bennett had successfully used. It is estimated that it would have been necessary to remove another 100 drawers to reduce the count rate sufficiently to make central measurements with the GE hydrogen counter with the halves closed. In view of the count-rate limit, a direct comparison of the performance of the equipment was not possible. Measurements were made with hydrogen and methane counters at the core center with the halves separated by 3 and 4 in. and with all 10 safety rods "out," and with a methane counter alone (higher energy end of the spectrum only) with halves closed. A complete set of measurements with both counters in the blanket was made with the halves closed and safety rods "in." The data are now being analyzed by GE at Vallecitos.

The reactor was reloaded to critical and additional spectrum-measuring experiments at the core center were conducted with the Li^6 semiconductor sandwich fast-neutron spectrometer. The results will be compared directly with the results of the proton-recoil measurements. The resolution of the system used was about 70 keV full width at half-maximum. Data reduction is currently underway.

The arrangement of core and blanket was then adjusted to give the reference critical configuration. In order to define the neutron spectrum in the assembly more completely and to enhance the comparison of calculated and measured spectra, fission ratios relative to U^{235} were measured with thin-walled aluminum, back-to-back fission chambers containing thermally intercalibrated foils of U^{233}, U^{234}, U^{236}, U^{238}, Pu^{239}, and Pu^{240}. For comparison, measurements were also made with heavy-walled (Kirn) counters containing foils having the same principal isotopes as above.

b. ZPR-6

(i) Experimental. Criticality was achieved with Assembly No. 5 of ZPR-6 (see Progress Report for June 1966, ANL-7230, p. 7) on July 8, 1966. The critical mass with a 22-cm-thick reflector of depleted uranium was 1590 kg of U^{235}.

In the calculations that were done for this core, a reflector thickness of 27 cm was used. With the use of cross-section set 224 a critical mass of 1591 kg had been predicted. However, this agreement may be

fortuitous for two reasons: (1) the radial reflector is 22 cm thick (preliminary experimental results indicate that addition of a 5-cm layer of depleted uranium to the reflector will reduce the critical mass by 10-20 kg of U^{235}), and (2) the atomic density of U^{235} in the outer radial ring (~12 cm thick) was 10-20% lower than that at the center of the core. This nonuniformity in the concentration of U^{235} in the core was unavoidable because of the variation in the weight per unit length of the U^{235} plates. Thus the final value of the critical mass must await the arrival of more depleted uranium and the evaluation of the effect of lower atomic concentration of U^{235} in the outer 12-cm shell.

The results of measurements of central worth are given in Table VIII. The central worth measurements from Assembly No. 4Z are also given in Table VIII. Assembly No. 4Z was a zoned version of Assembly No. 5, so that the ratio of the worth of a sample in Assembly No. 5 to that in Assembly No. 4Z should be constant for all samples provided the spectral matching of the real and adjoint fluxes is exact in both assemblies. It is seen from Table VIII that this ratio is near unity with fluctuations of about 6%. In the case of sodium, the signal is rather small and the 16% deviation is within the experimental uncertainty.

TABLE VIII. Central Worths in ZPR-6 Assembly No. 5

(1% $\Delta k/k$ = 476 Ih)

Sample and Wt (g)	Wt of Can (g)	Gross Worth (Ih)*	Net Worth (Ih)	Net Worth in Assembly 4Z (Ih)	Worth in Assembly 5 / Worth in Assembly 4Z: Measured	Worth in Assembly 5 / Worth in Assembly 4Z: Calculated by Set 224
Be (114.308)	Bare	+1.130 ± 0.048	1.130 ± 0.048	+1.107 ± 0.010	1.021	0.987
C (103.0)	Bare	+0.183 ± 0.022	+0.183 ± 0.022	+0.197 ± 0.010	0.943	1.080
Ni (546.0)	Bare	-1.134 ± 0.015	-1.134 ± 0.015	-1.148 ± 0.010	0.988	1.011
V (183.67)	55.30 (SS)	-0.246 ± 0.010	-0.136 ± 0.014	-0.133 ± 0.010	1.022	
Li (28.30)	57.03 (SS)	-0.790 ± 0.010	-0.677 ± 0.015	-0.595 ± 0.010	1.137	
Zr (406.0)	Bare	-0.671 ± 0.020	-0.671 ± 0.020	-0.650 ± 0.005	1.032	
Mo (599.0)	Bare	-3.416 ± 0.015	-3.416 ± 0.015	-3.415 ± 0.010	1.000	
Al (166.90)	Bare	-0.300 ± 0.017	-0.300 ± 0.017	-0.297 ± 0.013	1.010	
B^{10} (29.29)	55.73 (SS)	-23.298 ± 0.030	-23.400 ± 0.033	-23.339 ± 0.200	1.003	1.012
B_4C (59.62)	64.70 (SS)	-6.266 ± 0.010	-6.137 ± 0.015	-6.410 ± 0.025	0.960	
Poly. (58.98)	Bare	+19.122 ± 0.010	+19.122 ± 0.010	+19.696 ± 0.010	0.970	
Nb (481.2)	30.10 (SS)	-3.888 ± 0.010	-3.939 ± 0.015	-3.791 ± 0.010	1.039	
W (1108.0)	Bare	-5.792 ± 0.020	-5.792 ± 0.020	-5.742 ± 0.010	1.010	
Ta (924.70)	27.54 (SS)	-11.955 ± 0.010	-12.001 ± 0.015	-11.907 ± 0.200	1.008	
U^{238} (1153.80)	Bare	-3.869 ± 0.010	-3.869 ± 0.010	-3.857 ± 0.010	1.003	1.011
U^{235} (13.869)	48.968 (SS)	+0.545 ± 0.010	+0.648 ± 0.012	+0.611 ± 0.02	1.060	1.013
U^{235} (27.719)	SS can (47.30)	+1.174 ± 0.010	+1.278 ± 0.012	+1.246 ± 0.030	1.030	
U^{235} (64.183)	SS can (47.30)	+2.951 ± 0.010	+3.055 ± 0.012	+2.890 ± 0.030	1.057	
Na (51.38)	56.42 (SS)	-0.144 ± 0.008	-0.041 ± 0.010	-0.049 ± 0.005	0.840	1.003
SS 304 (499.6)	Bare	-0.851 ± 0.020	-0.851 ± 0.020	-0.849 ± 0.010	1.002	

*Some samples were encased in stainless steel (SS) cans.

A complete overhaul of the Kaman Nuclear pulsed neutron source became necessary because of breakdowns in the high-voltage system and insufficient vacuum in the accelerator. The vendor repaired the high-voltage supply and installed a new ion pump. Both components appear to be working satisfactorily now, but the system is still being tested. The vendor also manufactured a new, 5-ft 11-in.-long drift tube which was designed specifically to allow insertion into the $1\frac{7}{8}$-in.-dia hole extending

from the supporting knee on the side of ZPR-9 into the center of the matrix. In order to accommodate it in the available space, an air-cooled target assembly was chosen which will allow pulsing the beam at maximum intensity ($\sim 2 \times 10^{11}$ neutrons/sec) up to about 1% duty cycle. The 55 gal of transformer oil in the high-voltage supply were replaced by a silicone fluid in order to eliminate fire hazards.

(ii) Analysis. Calculations have been performed to check the suitability of the two-dimensional perturbation code PERT for calculations of the sodium void coefficient in Assemblies 2 and 3 of ZPR-6. PERT is a subroutine of the two-dimensional diffusion code CANDID. For four regions along the axis of Assembly No. 3 sodium void calculations with PERT were compared to one-dimensional infinite slab calculations with the perturbation code DEL (DEL is a subroutine of the one-dimensional diffusion code MACH 1). The PERT calculations were reduced to one dimension by introducing reflective boundary conditions in the radial direction. The results from the two codes which are comparable are: The leakage effect, the combined downscattering and capture effect, and the total effect. The results showed that the agreement between PERT and DEL is very dependent on the mesh arrangement used. For a very fine mesh (more than 100 points in one dimension) both codes appear to approach the same asymptotic results. When thirty mesh points are used with intervals of 1 to 1.5 cm in the core, the PERT results deviate from these asymptotic values by as much as 10%. Particularly sensitive is the leakage effect in the vicinity of the core-blanket boundary. The results of the DEL calculations are much less sensitive to the mesh spacing. Deviations of 10% from the asymptotic values appeared only when a very coarse mesh was used with 13 points and intervals of 2.5 to 3.7 cm in the core.

c. ZPR-9. Initial Doppler measurements made with Assembly No. 11 for natural and enriched 1/2-in.-dia UO_2 elements gave erratic results which were inconsistent with the precision of the measurements. Investigation showed that the auxiliary autorod-shim control rod system was at fault. The exact reason for the malfunction has not been determined. With the auto shim rod control system eliminated, consistent results were not only obtained with the natural-UO_2 sample for central worth measurements with Assembly No. 11 but also for results obtained with ZPR-6 Assembly No. 4Z. An investigation of the results for the enriched UO_2 sample is currently in progress.

d. ZPPR

(i) Status. The construction contract for the ZPPR facility was signed with Arrington Construction Company on July 28. Procurement of reactor components will be started again immediately. Bid packages were sent out for most of the procurement items during May and June. These bids have been received and are being evaluated.

The following is the present status of major reactor components:

(α) Reactor Bed and Tables. An ANL procurement representative visited the vendor's plant, Giddings and Lewis Machine Tool Company, Fond du Lac, Wisconsin, to observe progress being made on the bed and tables as well as component parts.

All materials required for the job, which were purchased from outside sources, have been received and are stored on pallets or in boxes in the small parts storeroom. The drive ball screw was returned from heat treating. The final machining of the ends for the bearings and drive gears has been started. The table castings are in the process of being cleaned and prepared for machining. The long runway casting is partially finished with the rough machining finished on the sides, top, and bottom. The short runway casting is also partially finished. Next the two runways will be fit together and machined as a unit. The vendor has set aside specific machines for exclusive machining of the ANL bed and tables, and work is progressing quite well.

(β) Matrix Drawers. Progress on the drawers by the vendor, Mechanical Products Mfg. Company, Seattle, Washington, has been slower than anticipated. Twelve hundred drawers have been formed and the front ends have been welded. The front end welds of these drawers are now being machine-finished. This operation at present is the holdup in the process.

(γ) Matrix Tubes. The matrix tubes have been stored at the vendor's plant and await shipping instructions.

(δ) Nuclear Instrumentation. Fabrication of the nuclear instrumentation is 61% complete.

(ϵ) Area Gamma Monitors. Fabrication of the area gamma monitors is 90% complete.

(ζ) Poison Safety Rod Drives. The bids have been evaluated and the approval package is being prepared for submission to the AEC.

(η) Reactor Knees. The bids have been evaluated and the approval package is being prepared for submission to the AEC.

(θ) Personnel Shields. This item was sent out to five vendors and no bids were received, primarily due to the short bidding period. These shields will be sent out again with a longer bidding period.

(ι) Tube Bundling. A re-evaluation of the necessity of tube bundling is in progress. It appears that an alternative method of installation of the tubes into the matrix assembly may be feasible and could result in a considerable savings to the project.

(ii) Safety Analysis. Two types of tests were run on the ZPPR fuel safety rods to determine the effect of imposing a.c. voltage on the holding magnets. In the first test, up to 130 V a.c. were applied directly to the latch magnet, with the normal d.c. latch power removed. With this a.c. voltage, it is not possible to latch the rod since the latch coils have sufficient inductive reactance to hold the alternating current value below that necessary to keep the magnet in the latch position. The d.c. magnets are designed to operate at 24 V.

In the second type of test, the d.c. latch power was applied and the rod driven to a normally inserted position with 130 V a.c. superimposed on the latch. The d.c. power was then removed and the rod scrammed normally. It is concluded that applications of a.c. line voltage will not degrade the normal scram functioning of the safety rod magnets.

Additional filtration tests with sand using uranine as the test aerosol are being performed.

5. Sodium Technology Development

a. Engineering Developments

(i) Component and Materials Evaluation Loop (CAMEL)

(α) Data-acquisition System. The data-acquisition system was operated to determine its operational characteristics. A condenser discharge voltage was recorded on the punched tape via the scanner. The voltage variation covered a wide range so that the autoranging characteristics were demonstrated to be operating properly. In addition, the printout of the data on the CDC-160A showed that compatibility of equipment exists. Also, the punched-tape data were processed on the programmable X-Y plotter and an accurate graphic reproduction of the data obtained. The equipment appears ready for use. The final wiring of the extension terminal of the acquisition system, which will permit programmable switching of the data acquisition system to alternate locations as desired, remains to be done.

(β) Modified Falex Materials Wear Tester. A second modified Falex wear tester has been assembled. This unit includes an improved feature which consists of an "outrigger" arm for the linear transformer and a bearing-mounted bridge moving along two parallel cantilever shafts, which results in a very smooth operation of the sensing mechanism.

A wear test, preliminary to testing in sodium, was started with the Falex tester in inert gas at 1200°F. The wear blocks were constructed of chill cast Haynes Stellite No. 19. The test shaft was constructed of 83% tungsten carbide, 8% titanium carbide, and 9% cobalt. The blocks were loaded to 660 psi and operated at a sliding velocity of 2.15 ft/min for a period of 14 hr. During this time, the indicated wear was equal to 0.0016 in. Seizing and erratic behavior were noticeably absent. The test is continuing.

b. Liquid Sodium Coolant Chemistry

(i) Carbon Analysis. The presence of carbon in sodium may be of significance in connection with carburization of stainless steel or other materials used as components in sodium systems. A new analytical method for the determination of carbon in sodium, developed for a range up to several hundred parts per million, utilizes potassium dichromate as an acidic oxidizing flux. Trapping of CO_2 by the sodium oxides produced in the oxidation is obviated by the acidic nature of the flux, which readily displaces CO_2 from Na_2CO_3.

A sodium sample and preignited flux are confined in a quartz bottle with a narrow opening at one end. The sodium oxide produced is prevented from retaining CO_2 by forced contact with the acidic flux. At temperatures around 800-900°C the acidic flux spontaneously decomposes, liberating oxygen which sweeps out both the melt and the bottle. The combustion products then enter the mainstream of oxygen and pass over a catalyst bed of platinum black supported on silica and then over a bed of CuO. The CO_2 is quantitatively produced from all the carbon in the sodium and is trapped out of the pure oxygen stream by a controlled-temperature cold trap. The trapped CO_2 is then flashed into a calibrated chromatograph for determination.

Carbon recovery tests using standard potassium acid phthalate gave good precision and complete recoveries, both with and without the presence of sodium.

Several analyses of sodium samples from the secondary sodium system at EBR-II gave good precision between aliquots from the same sample, i.e., from one sample, values of 11, 11, and 15 ppm carbon were observed, and 13, 15, and 14 ppm were found on another sample.

(ii) Segregation of Carbon in Sodium. A need to prepare ultrapure sodium for research purposes has led to studies of purification methods. Of the many methods examined for the removal of carbon, a zone-refining technique (see Progress Report for April 1966, ANL-7204, p. 31) has given the most encouraging results. A fused silica tube filled with sodium was subjected to zone refining for two months. The sodium at the end toward which the molten zone travelled contained less carbon than any other sodium thus far analyzed (3-4 ppm carbon). In addition, the sodium at or near the walls of the zone-refining tube contained substantially more carbon than the sodium in the core of the tube (80-90% of the original carbon was concentrated at or near the walls). In order to determine whether segregation of carbon would occur under conditions which differ from those of zone refining, two simple experiments were recently performed. In one, sodium at 165°C, containing 30-35 ppm carbon, was drawn up into a fused silica pipette and allowed to freeze. In the second, sodium, also at 165°C, was poured into a fused silica U-tube and allowed to freeze.[5] Sodium samples extruded from the core sections of the pipette and U-tube were analyzed for carbon. Two core samples from the pipette and one from the U-tube contained 13, 9, and 15 ppm carbon, respectively. A section of sodium near the wall of the U-tube was also analyzed and was found to contain more carbon than the core section. Significant segregation therefore occurred upon solidification. Since other experiments (centrifugation and filtration) showed that at least 40-50% (and perhaps more) of the carbon in the starting sodium was finely divided particulate material, the apparent segregation may be due to surface effects. Investigations aimed at isolating and characterizing these effects are currently under way.

These results clearly demonstrate that caution should be exercised when liquid sodium is sampled for carbon analyses by pipette methods. To avoid nonrepresentative analyses, the total sample, including sodium adhering to the walls of the pipette, should be analyzed. Otherwise, sampling methods in which surface effects are minimized should be used.

6. EBR-II

a. Operations. On the basis of the fuel surveillance following Run No. 19 (see Sect. I.A.7) the burnup limit for Mark-IA fuel was temporarily set at 1.2 a/o, since all subassemblies in the core contain some fuel pins fabricated in Argonne, Illinois.

Run No. 20-A, for the purpose of irradiating flux wires, was made on July 18 for one hour at 10 kW. The main reactor loading changes for this run consisted of two experimental subassemblies (XO13 and XO14, containing nonfissile reactor materials and structural samples), one experimental source, six flux wire subassemblies, and six fueled inner blanket subassemblies to compensate for the two experiments. On the following

[5]The pipette and U-tube had the same OD (10 mm) and were cleaned in the same manner as the zone-refining tube.

day, after removal of the flux wire subassemblies and their replacement with four core-type and two inner blanket subassemblies, Run No. 20, scheduled for 700 MWd, was begun. For this run, the reactor core contained 80 subassemblies, including eight experimental subassemblies and the stainless steel rod in a control rod position.

The flux wires from Run No. 20-A were counted, and the subassemblies were washed and reloaded for additional measurements in different grid locations for an equal irradiation period (Run 20-B). One grid location will be identical in both wire irradiations for normalizing the two runs. These data will give experimental verification of power and flux distribution in the 80-subassembly core containing 8 core-type experimental irradiation subassemblies.

The reactivity loss from criticality to full power of 45 MW was measured to be 74 Ih at the start of Run No. 20. Control rods 3 and 8 were calibrated by period measurement, the values being 123 and 158 Ih, respectively. The other control rods were calibrated by comparison, and the average values of odd and even control rods were 131 and 158 Ih, respectively.

A proposal for irradiating 70% enriched fuel pins in EBR-II at 45 MW has been prepared and is awaiting the results of low-power flux measurements before further action is taken on it. It is anticipated that a postirradiation inspection of the highly enriched pins will provide advance information relevant to the performance of Mark-IA fuel under operation at higher levels of power.

The proposal calls for the irradiation of 61 pin clusters in subassemblies with 30 normal driver fuel pins in Row 4 positions. The results of calculations indicate that conditions of specific power and coolant flow rate in Row 4 are such that maximum fuel and cladding temperatures are assured. With an inventory of 300 70% enriched pins on hand four complete 61 pin clusters can be assembled. Remaining pins will be assembled into a fifth unit which will be removed first for fuel surveillance purposes.

Calculations of fuel, bond, and cladding temperatures were carried out to establish conformity with the requirements of the Hazards Summary Report.

b. Maintenance and Modification. As a result of the noise and vibration that occurred in the generator during a routine overspeed-trip test of the turbine (see Progress Report for June 1966, ANL-7320, pp. 1-2), the generator was disassembled and inspected. One of the rotating field connection box covers had broken loose and struck the stator. The end of one stator winding loop sustained minor damage to insulation and copper

wires. The bottom half of the forward generator bearing (closest to the turbine) was found "wiped" and the babbit was cracked in one place. Because of the appearance of this bearing and the adjacent bearing on the turbine, alignment was checked and revealed that the generator was about 0.015 in. high with respect to the turbine. The cause of the misalignment has not been determined. A representative from General Electric, the vendor that installed the machine, is on the site, repairs are in progress, and the generator will be reassembled as soon as the repairs are made.

c. Reactor Improvements

(i) Core Subassembly, Models SRB and STB. The original design and construction of the core subassemblies provided an axial blanket section above and below the fuel elements, consisting of eighteen depleted-uranium elements. In order to reduce both the assembly and material costs, stainless steel rods were used in Model SRB instead of the depleted uranium. The Model SRB subassemblies are presently being used in the reactor.

Because each blanket section, at present, consists of two grids, eighteen blanket elements, one spacer, and one nut, considerable assembly time is required. Therefore, in order to further reduce costs, a new design, Model STB (see Fig. 2), has been completed. The upper blanket consists of a single triflute configuration made of stainless steel, the lower blanket section of an identical stainless steel triflute with a flow distributor located at the upper end to provide uniform sodium flow into the fuel-element support grid.

Prototype components of the Model STB were fabricated. Hydraulic flow tests have established the proper dimensions to match the hydraulic characteristics of the present subassemblies. The results, based upon the effective pressure drop of a 67-subassembly core configuration, are shown in Table IX.

Model STB subassemblies should be ready for use in approximately six months.

(ii) Oscillator System, Mark II. The oscillator-system tests continued with operation of the rod for 27 hr at speeds up to 600 rpm. Although no difficulties had been experienced during prolonged runs at speeds of 300 rpm, the drive-shaft torque readings showed an increase at higher speeds, and the higher-speed tests were stopped to investigate the reason for the high torque readings.

The drive shaft was removed from the sodium test vessel and disassembled for inspection. The two lower drive-shaft bearings, which were immersed in sodium, were scored. This bearing condition will be investigated before the tests are continued.

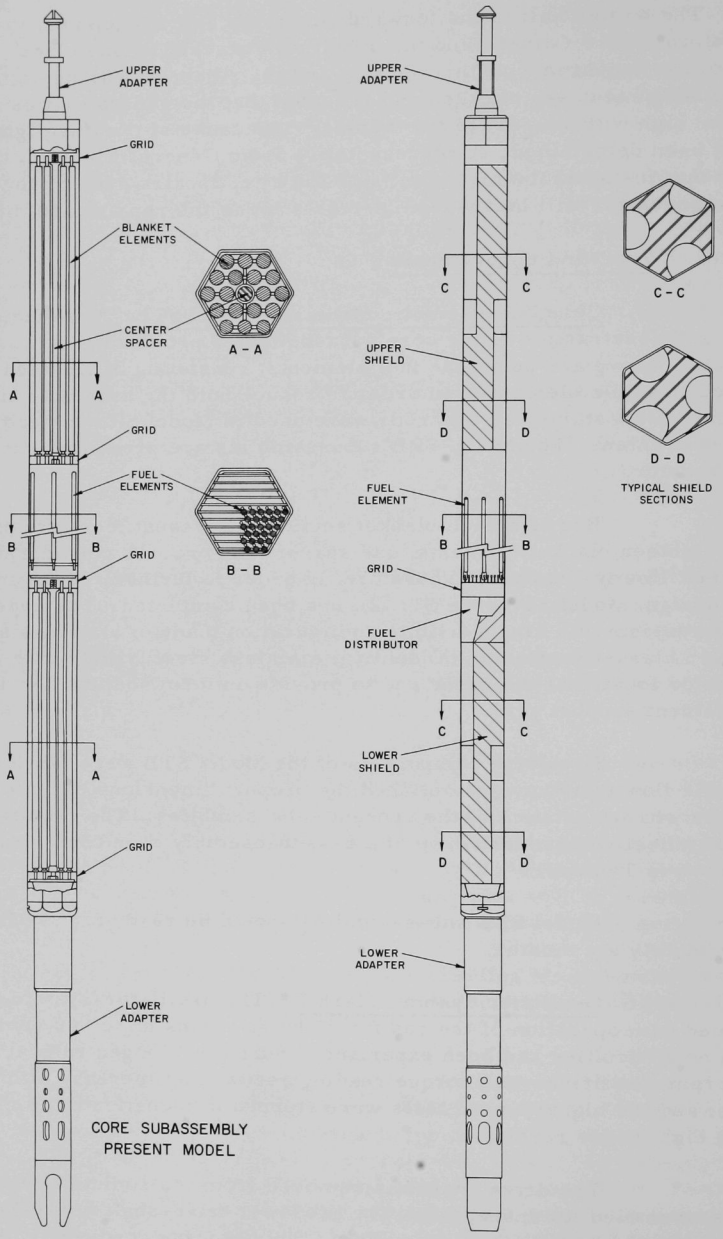

Fig. 2. Core Subassembly--Model STB (Stainless Triflute Blanket)

TABLE IX. Flow-test Results of the EBR-II Core Subassembly Model STB

Reactor Row	Effective Pressure Drop (psi)	Flow of 800°C Sodium (gpm)		
		Franklin Institute Data*	Present Core Subassembly**	STB Core Subassembly
1, 2	38	139	142	141
3	39	123	123	124
4	34.5	93	89	91
5	34	78	74	77

*Results obtained by the Franklin Institute from tests conducted in 1960.
**Results obtained from a production core subassembly test performed just prior to the final tests of the Model STB subassembly.

A proposal was made to eliminate the number 4 bearing in the oscillator rod. Computer results for the critical speed of EBR-II oscillator rod indicate that if the number 4 bearing is eliminated, the critical speed is reduced to about 250 rpm, which is far less than the operating speed.

(iii) Structural Materials Irradiation Subassembly. The final design studies of a nineteen-element configuration-type subassembly were completed. The element size (0.493 in. in dia) met the requirements for specimens as set by the experimenters. Generally, the elements of the irradiation subassembly would be similar to those in the outer blanket subassemblies.

During design layout stages, further studies and discussions indicated that an arrangement by which three irradiation capsules would be inserted into each of the seven elements of the Mark B-7 Irradiation Subassembly is acceptable. This approach will eliminate the cost of developing, detailing, testing, and fabricating special hardware as the Mark B-7 Irradiation Subassembly has been completed (see Progress Report for April 1966, ANL-7204, pp. 2-3).

(iv) Irradiation Subassembly Mark C. Detailed drawings for the Irradiation Subassembly Mark C are being prepared. This subassembly will allow higher temperature rises of the coolant than possible by bypassing a portion of the coolant flow around the test elements. The bypass flow channel is formed by the standard size outer hexagonal enclosure and a smaller inner hexagonal enclosure which surrounds the test elements. The initial construction will have nineteen elements spaced with spiral wires. A maximum exit temperature of sodium from the test elements of 1200°F

appears possible based on calculations. The mixing area above the elements is used to mix the hot (1200°F) sodium with the cooler bypass sodium to match the exit temperature with that of adjacent core subassemblies in the reactor. Orificing is provided to control total and bypass flows.

(v) Control Rod, Model IHE. During unrestricted fuel handling, when the control rod drives are disconnected from the rods and raised, and the reactor vessel cover is raised and rotated from its "operate" position, no overhead obstructions are present to prevent upward movement of the control rods. Under these conditions, the total holddown force on each rod is equal to its weight in sodium. Theoretically, if both primary pumps then were somehow started, a hydraulic lifting effect would develop which would reduce the total holddown force; shortly before full reactor flow was reached, the control rod weight would be offset by the hydraulic lifting force and the rods would rise. Although there are multiple interlocks to prevent pump operation during such conditions, an additional safety factor results from a control rod design that prevents rod motion even if flow occurs accidentally.

A new bushing on the lower part of the control subassembly located between the two existent bushings has been added. The new bushing enters the smaller diameter portion of the guide tube when the control subassembly is at the lower portion of its stroke. A very slight reduction in the outside diameter of the upper bushing (0.004 in.) is required to supplement the effect of the new bushing. This decrease in diameter increases the upward flow between the control subassembly and its guide tube in the raised position from about 5 to about 7 gpm, which reduces the tendency to build up a lifting force on the upper bearing.

d. Reactor Physics

(i) Pressure-pulse Studies. From time-temperature values from ARGUS calculations and a physical model, the shape of the pressure pulse resulting from a failure in the region of the gas space in a Mark-IA fuel pin was established. Based on an estimate of the associated energy release and an estimate of the energy required for permanent damage to the hexes, permanent deformation of the hexes in the event of such a failure appears unlikely.

A physical model for the situation in which one or more fuel pins fails under blocked coolant flow conditions is being formulated. Generalized differential equations relating time, temperature and pressure are being set up for machine programming. By assuming an arbitrary but realistic rate of molten fuel extruding into stagnant sodium, it will be possible to estimate the time dependence and the magnitude of the resulting pressure pulse.

e. Experimental Irradiations. The status of all experimental irradiations in the grid at month's end are listed below:

Subassembly	Date Loaded	Accumulated Exposure (MWd)	Goal Exposure (MWd)	Experimenter
XG02	7/16/65	6567	13,600	GE
XG03	7/16/65	6567	19,450	GE
XG04	7/16/65	6567	39,000	GE
XG05	9/3/65	6140	10,300	GE-ANL (MET)
XG06	9/3/65	6140	20,600	GE-ANL (MET)
XA07	10/27/65	5403	18,600	ANL (MET)
XA08	12/13/65	4318	19,800	ANL (MET)
XO04	3/24/66	3498	5,130	UNC, ANL (MET), GE, PNWL
XO10	3/24/66	3498	19,600	ANL (MET), GE, PNWL
XO11	5/9/66	1927	8,300	ANL (MET), GE, PNWL
XO13	7/17/66	497	1,200	ANL (MET), PNWL
XO14	7/17/66	497	-*	PNWL, NRL, GE
U-1548X	5/6/65	7438	6,080**	ANL (CEN)
U-1549X	5/6/65	7438	6,080**	ANL (CEN)
U-1550X	5/6/65	7438	9,120**	ANL (CEN)
U-1551X	5/6/65	7438	9,120**	ANL (CEN)

*Maximum attainable before core has reached terminal size.
**Minimum acceptable.

f. Fuel Cycle Facility

(i) Fuel Surveillance. Continued surveillance of the Mark-IA fuel has shown a difference between Chicago-manufactured and FCF-manufactured fuel. In addition to those previously reported (see Progress Report for June 1966, ANL-7230, pp. 3-5), sodium-level measurements were made of one Chicago-manufactured Mark-IA subassembly (C175--1.22 a/o max burnup) and one irradiated subassembly containing both FCF and Chicago-produced fuel (C179--1.22 a/o max burnup). The change in volume of the fuel from C175 was 14%, approximately the same as that previously obtained from Chicago fuel of comparable burnup. Measurements with C179 showed that the 25 FCF-produced elements had an average volume increase of about 8%, whereas the 19 Chicago-produced pins had an average volume increase of 13%. Measurements of pressure and void volume made on the void space in the top of elements from these subassemblies

confirmed both the relatively high fuel volume increases and the differences between the fuels of the two sources. The reason for these high values and for the differences in these values is not yet known. Additional surveillance will be made on other subassemblies to help define these differences.

(ii) Plutonium in Blanket Material. Plutonium has been determined in samples of axial blanket rods obtained from subassemblies in which the maximum fuel burnup ranged from 0.27 to 1.2 a/o. The amount in samples obtained from the end near the core ranged from 204 to 1144 μg Pu/g U. As would be expected, a considerably lower concentration was found in the end away from the core. Values are shown in the following table:

Plutonium in Axial Blanket Samples

Subassembly No.	Max Fuel Burnup (a/o)	Blanket Section	Sample Location	Total Pu (μg/g U)
C-140	0.27	Upper	Bottom	204
C-143	0.50	Upper	Bottom	440
C-104	1.21	Lower	Top	1144
C-104	1.21	Lower	Bottom	138

(iii) Production. A summary is given in Table X.

TABLE X. Production Summary for July 1966

Subassemblies received:		13 plus 4 foil assemblies
Subassemblies dismantled:		17
Subassemblies fabricated:		9
Subassemblies transferred to reactor:		9
Pins decanned:		1361
Melt refining:	9 irradiated	7 recycle
Pour yield (avg %):	92.6	93.1
Injection-casting runs:		7
Pin processing:		
Accepts		654
Rejects		78
Pins welded:		692
Leak testing:		
Accepts		839
Rejects		7
Bond testing: (complete runs)		
Accepts		1064
Rejects		254
Surveillance:	C175, C179, C206, C209	

II. GENERAL REACTOR TECHNOLOGY

A. Applied and Reactor Physics Development

1. ARC System

a. Resonance Interference. A versatile and precise method of computing effective resonance cross sections for epithermal energies is being developed. Because the method is not based on the assumption of a "$1/E$" or a "$1/\Sigma$" flux, it includes the effect of flux perturbation and interference among resonance on effective cross sections. Also, because restrictions are not placed on the regional cross sections, it allows for resonances in the moderator and nonuniform temperature distributions in the fuel. Other methods,[6-9] aside from Monte Carlo programs, are either unwieldy or restricted to two regions with resonances only in the fuel rod. The new method, which is well suited for incorporation into the ARC system, can treat either slab or circularized cells.

The reactor cell is divided into thin slabs or annuli as in the THERMØS code.[10] The energy range of interest is divided into broad groups that are subdivided into many fine groups of equal lethargy width. The width of a fine group, Δu, is taken to be much smaller than the maximum lethargy gain per collision with uranium, so it is valid to assume that a neutron has only one collision in a fine group. From the slowing-down source S_{ij} into fine group j in region i, the first flight transmission and escape probabilities, the interface currents, and the collision rate C_{ij} is obtained. The reaction rate for process z (fission, absorption, or scattering) for material m is simply

$$ {}_zR_{ij}^{m} = {}_z\Sigma_{ij}^{m} C_{ij}/\Sigma_{ij}, \qquad (1) $$

---

[6]Driggers, F. E., A Method of Calculating Flux Spectra and Neutron Absorptions at Epithermal Energies, Trans. Am. Nuc. Soc. 8, 206 (1965).

[7]Adler, F. T., and Lewis, E. E., Comparison of Exact and Approximate Treatments of Resonance Effects in Cylindrical Lattices, Trans. Am. Nuc. Soc. 7, 29 (1964).

[8]Stevens, C. A., and Joanou, G. D., Investigation of the Flux Recovery Assumption in Resonance Computations, Trans. Am. Nuc. Soc. 8, 287 (1965).

[9]Kier, P. H., RIFF-RAFF, A Program for Computation of Resonance Integrals in a Two-region Cell, ANL-7033 (1965).

[10]Honeck, H. C., A Thermalization Transport Theory Code for Reactor Lattice Calculations, BNL-5826 (1961).

where ${}_z\Sigma_{ij}^m$ is the macroscopic cross section for the process and Σ_{ij} is the total macroscopic cross section. The reaction rates are accumulated over the broad group to obtain either resonance integrals or effective cross sections.

For the case of a circularized cell, cosine interface currents are assumed. Then the collision rates can be obtained in terms of the following quantities:

J_i^+ ≡ cosine current impinging on the inner surface of the region i + 1;

J_i^- ≡ cosine current impinging on the outer surface of the region i;

P_i^+ ≡ escape probability through outer surface of region i for flat volume source;

P_i^- ≡ escape probability through inner surface of region i for flat volume source;

T_i^{OI} ≡ transmission probability from inner to outer surface of region i;

T_i^{IO} ≡ transmission probability from outer to inner surface of region i;

T_i^{OO} ≡ transmission probability from outer to outer surface of region i.

Expressions for these transmission and escape probabilities are given in Ref. 9. The collision rates are

$$C_{ij} = \begin{cases} (1 - T_i^{OO}) J_i^- + (1 - P_i^+) S_{ij} \text{ for } i = 1 \\ (1 - T^{OI}) J_{i-1}^+ + (1 - T_i^{OO} - T_i^{IO}) J_i^- + (1 - P_i^+ - P_i^-) S_{ij} \text{ for } i = 2,I. \end{cases} \quad (2)$$

The interface currents are obtained from the system of equations representing neutron conservation at the interfaces and isotropic return at the outer surface of the cell:

$$J_i^+ = \begin{cases} T_i^{OO} J_i^- + P_i^+ S_{ij} \text{ for } i = 1 \\ T_i^{OI} J_{i-1}^+ + T_i^{OO} J_i^- + P_i^+ S_{ij} \text{ for } i = 2,I, \end{cases} \quad (3)$$

and

$$J_i^- = \begin{cases} T_{i+1}^{IO} J_{i+1}^- + P_{i+1}^- S_{i+1,j} & \text{for } i = 1, I-1' \\ J_i^+ & \text{for } i = I. \end{cases} \tag{4}$$

The sources for a fine group are assumed to be constant within a region but are allowed to vary from region to region. The neutron source has the following form:

$$S_{ij} = \sum_{m=1}^{M} \sum_{k=1}^{K_m} P_{km} \Sigma_{s_{j-k,m}} \phi_{i,j-k} \tag{5}$$

where P_{km} is the probability that a neutron is scattered down k groups in a scattering collision with material m, $\Sigma_{s_{j-k,m}} \phi_{i,j-k}$ is the scattering rate, and K_m is the maximum number of groups through which a neutron can be scattered. Equation (5) would be prohibitively time-consuming to evaluate because a neutron can be scattered through so many groups. However, use of groups of equal lethargy width and the assumption of elastic scattering permit Eq. (5) to be reduced to the much more suitable form:[9]

$$S_{ij} = \sum_{m=1}^{M} P_{1m} \Sigma_{s_{j-1,m}} \phi_{i,j-1} + e^{-\Delta u} \left\{ S_{i,j-1} - \sum_{m=1}^{M} P_{K_m'm} \Sigma_{s_{j-K_m-1,m}} \phi_{i,j-K_m-1} \right\}. \tag{6}$$

B. Fuels and Cladding Materials

1. Th-U-Pu Alloys

The thorium-uranium-plutonium alloys are being studied to determine their usefulness as fast reactor fuels. The alloys Th-10 w/o U-10 w/o Pu and Th-20 w/o U-10 w/o Pu have the best combination of properties for use as fuels and the properties are being measured on these alloys. These alloys have very high thermal conductivity (see Table XI) and about the same values. The thermal conductivity was measured in a comparative apparatus with an Armco iron standard.

TABLE XI. Thermal Conductivity (W/cm-°C) of Th-10 w/o U-10 w/o Pu and Th-20 w/o U-10 w/o Pu Alloys

Temp (°C)	Th-10 w/o U-10 w/o Pu	Th-20 w/o U-10 w/o Pu	Temp (°C)	Th-10 w/o U-10 w/o Pu	Th-20 w/o U-10 w/o Pu
100	0.264	0.250	500	0.327	0.324
200	0.283	0.271	600	0.334	0.336
300	0.300	0.291	700	0.341	0.344
400	0.315	0.309	800	0.346	0.348

2. Heat Content of U-15 w/o Pu-6.5 w/o Ti Alloy

The heat content of the U-15 w/o Pu-6.5 w/o Ti alloy was measured in a drop calorimeter up to 1150°C, to support calculations for investigating the use of this fuel alloy in a fast reactor.

The increase in heat content is almost linear from 25 to 500°C and from 850 to 1150°C (see Fig. 3). Between 550 and 850°C the heat released by the three phase transformations produce a rapid rise in the enthalpy curve and is about equal to the $\alpha \rightarrow \beta$, $\beta \rightarrow \gamma$, and $\gamma \rightarrow$ liquid heats of transformation in unalloyed uranium. A good portion of the total rise in the enthalpy curve is undoubtedly due to the heat of formation of the compound U_2Ti. From the ternary phase diagram, one would expect that the curve should be discontinuous at 575, 650 and 655°C, the temperatures of the four-phase reactions in the system. However, only three calorimeter drops were made in the 550 to 850°C region and the curve could not be accurately described.

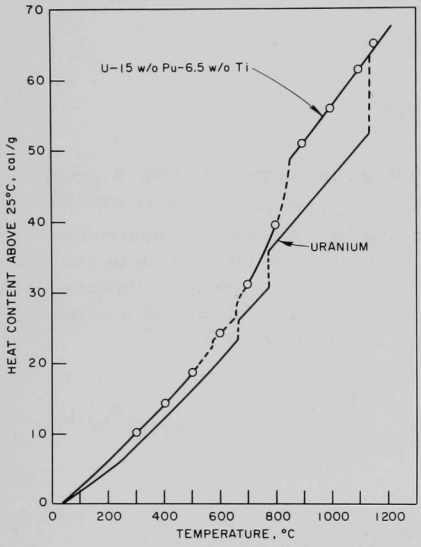

Fig. 3. Heat Content of U-15 w/o Pu-6.5 w/o Ti Alloy above 25°C

A parabolic equation was developed from the heat-content data of the alloy. An excellent fit to the data was obtained by calculating for the regions 25 to 550°C and 850 to 1150°C separately. The maximum deviation between observed and calculated values was about 0.5%. The equations for heat content and specific heat in the two temperature regions are:

$$\Delta H_{25},\ 25 \text{ to } 550°C = -0.7 + 0.0324T + 0.0000126T^2 \pm 0.5 \text{ cal/g}$$

$$850 \text{ to } 1150°C = 57.1 - 0.0531T + 0.0000521T^2 \pm 0.5\% \text{ cal/g};$$

$$C_p,\ 25 \text{ to } 550°C = 0.0324 + 0.0000252T \text{ cal/g/°C}$$

$$850 \text{ to } 1150°C = 0.0531 + 0.0001042T \text{ cal/g/°C}.$$

The total heat effect in the transformation region from 550 to 850°C is 28.7 cal/g.

3. Mechanical Properties of Uranium Compounds

The data for fracture tests of UO_2 at 1750°C with variations in strain rate are shown in Fig. 4. The specimens used in these experiments were of a higher density than those used previously, and there is an indication the maximum stress is dependent on the density in the brittle ductile range. Density measurements taken before and after test revealed changes of <1%. Density changes of from -0.56 to +0.66% were observed on specimens tested at various temperatures. This small change in density compared with prior observations could be caused by the longer equilibrating heat treatments given these specimens.

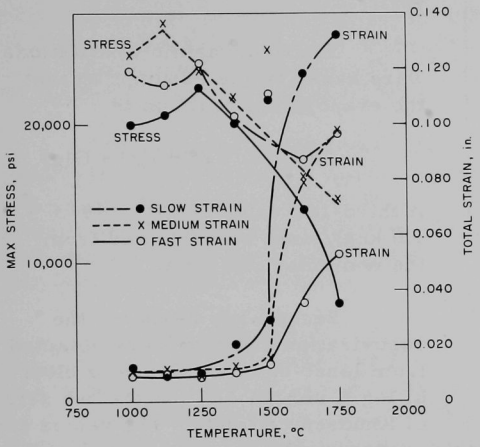

Fig. 4. Maximum Stress vs. Temperature and Total Strain vs. Temperature for UO_2

4. Thermal Stability of Plutonium Ceramics

a. Glovebox Testing. Leak-checking of the thermogravimetric analysis glovebox was completed. The glovebox is now closed and ready for plutonium experiments. Evaporation runs on PuO_2 will be started soon.

b. Gd_2O_3 Evaporation. Analysis of the Gd_2O_3 evaporation data (see Progress Report for June 1966, ANL-7230, p. 35) was completed. Figure 5 shows the collected weight-loss data and the lines passing through the three sets of data points derived from least-squares fits obtained with use of the IBM 3600 computer. Equations that fit the data are

$$\log_{10} m = 10.021 \pm 0.362 - \frac{(34.855 \pm 0.812) \times 10^3}{T} \text{ (Langmuir)};$$

$$\log_{10} m = 8.504 \pm 0.480 - \frac{(31.255 \pm 1.206) \times 10^3}{T} \text{ (Cell No. 1)};$$

$$\log_{10} m = 8.504 \pm 0.161 - \frac{(31.417 \pm 0.398) \times 10^3}{T} \text{ (Cell No. 2)},$$

where m is the weight-loss rate ($gcm^{-2}sec^{-1}$) and T is the absolute temperature (°K).

Two of the main purposes of the Gd_2O_3 work were to calibrate the apparatus and to perfect the measurement techniques: it is therefore

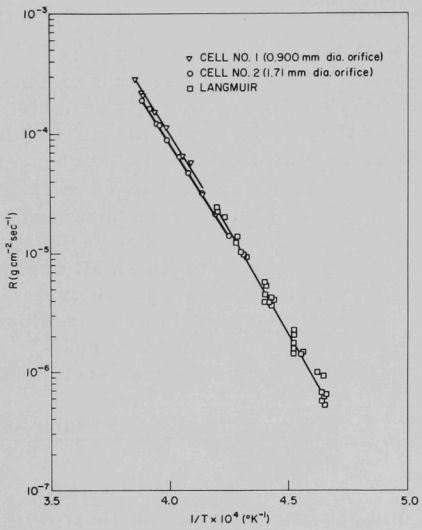

Fig. 5. Collected Evaporation-rate Results for Gd_2O_3

encouraging to note the good agreement between the two sets of cell data. The Langmuir and Knudsen data also agree in the region of overlap. The agreement of all the data is also significant in that it indicates an evaporation coefficient of unity.

Thermodynamic calculations were based on the assumption that the evaporation reaction is

$$Gd_2O_3(s) = 2GdO(g) + O(g).$$

A third-law value of $\Delta H_0^\circ = 464.0 \pm 1.0$ kcal/mole was obtained from the combined cell data.

Second-law heats for the vaporization reaction were obtained from least-squares slopes of plots of log K versus 1/T for the two sets of Knudsen cell data. The values are 436.6 ± 16.6 and 438.8 ± 5.3 kcal/mole, respectively, for cells Nos. 1 and 2. Third-law heat values, for the average temperature for each series, were calculated from the entropy data of White et al.[11] These are 437 and 439 kcal/mole, respectively, for cells Nos. 1 and 2. That the values are in good agreement lends additional confidence in the measurement procedure.

5. U-S-O System

The compound UOS can be readily synthesized by reacting approximately equimolar mixtures of UO_2 and US_2 at 1200°C in vacuum. Compositions near to UOS lying on the UO_2-US_2 and U_3O_8-US_2 joins were examined to secure information on the homogeneity range of UOS.

Six compositions in the range from $UO_{1.05}S_{0.95}$ to $U_{0.93}S_{1.07}$ were blended from UO_2 and US_2 powders, pelletized, fired at 1650°C for 3 hr in vacuum, and analyzed by X-ray and metallographic techniques. Exact conclusions must await the receipt of chemical analyses, but some general observations can be made. All specimens from $UO_{1.05}S_{0.95}$ to UOS contained 2 to 3 v/o of small yellowish US particles dispersed in a moderately dense,

[11] White, D., Walsh, P. N., Ames, L. L., and Goldstein, H. W., Thermodynamics of Vaporization of the Rare-earth Oxides at Elevated Temperatures, Thermodynamics of Nuclear Materials, pp. 417-443 (IAEA, Vienna, 1962).

light-gray UOS matrix, suggesting that the UOS was not stoichiometric but had an oxygen content less than that of U or S with a small range of variance for the sulfur. As further sulfur was added, a eutectic mixture consisting of a light-gray and a blue-gray phase appeared in increasing amount at the grain junctions as the US assumed a filamentary habit on the boundaries in decreasing amount. X-ray powder patterns indicated that the compositions were progressing into the US-UOS-U_3S_5 composition triangle with the reportedly stable U_2S_3 phase apparently nonexistent under the experimental conditions. The blue-gray phase must then be identified as U_3S_5, which forms a eutectic with UOS below 1650°C. The US-UOS and US-UOS-U_3S_5 eutectics must occur above this temperature.

The cell size of UOS was almost constant in this series, the lattice parameters for tetragonal, apparently sulfur-saturated UOS (from the $UO_{0.95}S_{1.05}$ composition) being determined as a_0 = 3.844 Å and c_0 = 6.694 Å. Results from a series of U_3O_8-US_2 mixtures indicated that oxygen-saturated UOS has a slightly decreased cell size, and thus UOS has at least a short homogeneity range for oxygen.

The U_3O_8-US_2 series covered the range of compositions from $UO_{1.51}S_{0.87}$ to $UO_{1.17}S_{1.12}$ and was fired at 1200°C for 3 hr in vacuum. A violent outgassing shattered the pellets at somewhere under red heat and all compositions ended up in the UO_2(SS)-UOS(SS) two-phase area. Calculations based on the following reaction sequence to give excellent agreement with the observed weight losses and quantitative phase distributions:

(1) $U_3O_8 + US_2 \rightarrow US_3 + UO_2 + US_2$
(2) $US_3 \rightarrow US_2 + S$
(3) $US_2 + UO_2 \rightarrow UOS$

} equations are unbalanced.

The oxidation characteristics of γUS_2, βUS_2, αUS_2, and UOS were compared to those of US in flowing oxygen in the DTA apparatus. The disulfides and US showed similar reaction sequences, the first reaction being very strongly exothermic, the sulfide being oxidized to UO_2(S) [the (S) here indicating a certain, considerable amount of sulfur retained in the UO_2 structure]; the second reaction, which is much more weakly exothermic at about 540°C, involves oxidation of UO_2(S) to U_3O_8(S), and the third is a weakly endothermic at 770°C, where the U_3O_8(S) decomposes to U_3O_8 + S. The oxidation resistance of the disulfides increased with the temperature stability of the polymorph, the strong exotherm occurring at 300°C for γUS_2, at 315°C for βUS_2, and at 375°C for αUS_2 as compared with about 400°C for US. UOS oxidized directly to U_3O_8(S) and this did not occur until about 540°C, with the retained sulfur again being liberated at 770°C.

6. Corrosion in Lithium at Elevated Temperatures

Study of the effect of metallic additives on lithium corrosion of tantalum at 1200°C has continued.

Yttrium is one of the known deoxidizing agents for lithium. The effect of yttrium on the lithium corrosion of tantalum is therefore of interest. However, the solubility of yttrium in lithium at the temperature of interest is not available.

A recent test indicated that yttrium is not compatible with lithium at high temperatures. At 1200°C, pure yttrium disintegrated in lithium in seven days. A dark-gray crust was formed on the inner surfaces of the tantalum test capsule. This coating was soluble in dilute acid, but not in water nor alkaline solutions.

A 2.5 a/o Y addition to lithium showed no beneficial effect on corrosion of tantalum at 1200°C. Instead, moderate acceleration resulted, as judged by comparison with a control sample (tantalum in lithium with no additive) tested under identical conditions. No layer was observed under metallographic microscope inspection after the acid dissolution treatment. Microhardness measurements indicated there was a slightly hardened layer at interior surfaces in contact with liquid as compared with vapor phase surfaces of the same capsule. This may indicate diffusion of impurities to the solid surface from the liquid.

A eutectic is formed in the Li-Na system at 170.6°C (3.4 a/o Na). The corrosion behavior of this composition toward refractory metals at the temperature of interest (1200°C) has not been investigated. An attempt was made to observe the effect of sodium on lithium corrosion of tantalum.

A tantalum capsule was used in this test. Results revealed that the eutectic composition induced some cracking of the sample. The corrosion attack on tantalum was highly accelerated as compared with that of pure lithium. Neutron radiographic inspection showed that the insert tantalum sample remained in the capsule vapor space which is proportionately richer in sodium than the liquid. No weight change or cracking of the insert sample was observed.

The vacuum distillation process for determination of oxygen in lithium showed little promise because it was very difficult to protect the apparatus from lithium attack at operating temperatures. A liquid ammonia process is now being investigated. Apparatus constructed in this laboratory has been assembled. Preliminary runs to establish routine procedures are now in progress.

7. Irradiation Testing

Ceramic fuel materials being developed under the high-temperature materials program are being irradiated in instrumented capsules in the MTR. A summary of the irradiations is shown in Table XII.

TABLE XII. Status of Ceramic Fuel Irradiations in Progress in MTR

		Design Parameters					Operating Conditions			
									Burnup to Date	
Capsule or S/A No.	Specimen Number	Fuel Composition (w/o)	Effective Density (%)	Cladding Composition (w/o)	Cladding OD (in.)	Cladding Thickness (in.)	kW/cc[a]	Max Clad Temp (°C)	a/o (U + Pu)	fiss/cc x 10^{-20}[a]
56-11	MV-2	UC-20 PuC	79	Nb-1Zr	0.281	0.012	1.2	470	5.6	14.4
56-8	MV-3	UC-20 PuC	81	Nb-1Zr	0.281	0.012	1.2	715	6.1	16.1
56-8	MV-5	UC-20 PuC	80	Nb-1Zr	0.281	0.012	1.2	705	5.8	15.2
56-11	MV-6	UC-20 PuC	80	Nb-1Zr	0.281	0.012	1.2	480	6.1	15.9
56-13	Z-4	UC-20 PuC	79	Nb-1Zr	0.174	0.015	1.2	665	1.0	2.6
56-13	Z-5	UC-20 PuC	79	Nb-1Zr	0.174	0.015	1.2	585	1.0	2.6
56-13	Z-7	UC-20 PuC	79	Nb-1Zr	0.174	0.015	1.2	570	1.0	2.6
56-13	C-45	PuC	84	Nb-1Zr	0.174	0.009	1.4	700	1.0	2.7
56-8	S-7	US	80	Nb-1Zr	0.281	0.012	1.0	535	4.4	8.5
56-8	S-8	US	89	Nb-1Zr	0.281	0.012	1.0	725	6.4	13.8
56-8	S-9	US	76	Nb-1Zr	0.281	0.012	1.0	750	6.4	11.7
56-8	S-10	US	91	Nb-1Zr	0.281	0.012	1.0	690	6.4	14.1
56-11	S-15	US	82	Nb-1Zr	0.281	0.012	1.0	380	3.5	6.9
56-11	S-16	US	90	Nb-1Zr	0.281	0.012	1.0	510	5.4	11.7
56-11	S-17	US	88	Nb-1Zr	0.281	0.012	1.0	500	4.1	8.7
56-11	S-18	US	77	Nb-1Zr	0.281	0.012	1.0	610	5.9	11.0

[a]Based on effective density.

C. Radiation Damage to Structural Materials

1. Fast-neutron Irradiation of Jacket Materials

The effects of fast-neutron irradiation and elevated temperature on the mechanical properties of Type 304 stainless steel, Hastelloy-X, Inconel-625, V-20 w/o Ti, and V-15 w/o Ti-7.5 w/o Cr are being investigated in the exposure range from 1×10^{21} to 1×10^{23} n/cm^2 and the temperature range from 550 to 750°C. Twenty-six capsules, containing 60 tube-rupture specimens and 296 tensile-type specimens, are being irradiated in EBR-II subassemblies XA07, XA08, XO09, and XO10 at temperatures between 500 and 670°C. The specimens have accumulated maximum total neutron exposures in the range from 6.3×10^{21} to 2.7×10^{22} n/cm^2.

Eighteen additional capsules containing a total of 117 tensile-type specimens were loaded into EBR-II subassembly XO13 for irradiation to 5×10^{21} n/cm^2 at a temperature of 650°C and have accumulated a maximum total neutron exposure of 3.0×10^{21} n/cm^2. The status and identification of the capsules are given in Table XIII.

TABLE XIII. Status of Cladding-materials Irradiations in EBR-II

S/A No.	Capsule Number	Design Parameters: Cladding Composition (w/o)	Type of Specimen	No. of Specimens	Specimen Environment	Operating Conditions: Max Specimen Temp (°C)	Exposure to Date (n/cm^2)
XA07	AS-9	V-20 Ti	Tensile	16	Argon-helium	590	2.7×10^{22}
XA07	AS-10	Hastelloy-X	Tensile	16	Argon-helium	590	2.5×10^{22}
XA07	AS-11	304 SS	Tensile	16	Argon-helium	590	2.6×10^{22}
XA08	AS-1	V-20 Ti	Tube-burst	12	Argon-helium	540	2.1×10^{22}
XA08	AS-2	V-20 Ti	Tube-burst	12	Argon-helium	540	2.1×10^{22}
XA08	AS-3	Hastelloy-X	Tube-burst	12	Argon-helium	540	2.2×10^{22}
XA08	AS-4	Hastelloy-X	Tube-burst	12	Argon-helium	540	2.2×10^{22}
XA08	AS-5	304 SS	Tube-burst	12	Argon-helium	540	2.2×10^{22}
XA08	AS-6	V-20 Ti	Tensile	16	Argon-helium	580	2.3×10^{22}
XA08	AS-7	Hastelloy-X	Tensile	16	Argon-helium	580	2.1×10^{22}
XA08	AS-8	304 SS	Tensile	16	Argon-helium	580	2.1×10^{22}
XA08	AS-12	V-20 Ti	Tensile	16	Argon-helium	580	2.0×10^{22}
XO09	AS-14	V-20 Ti	Tensile	13	Argon-helium	670	1.8×10^{22}
XO09	AS-15	V-20 Ti	Tensile	13	Argon-helium	670	1.7×10^{22}
XO09	AS-27	304 SS Hastelloy-X	Tensile	13	Argon-helium	670	1.9×10^{22}
XO10	AS-16	V-20 Ti	Tensile	13	Argon-helium	500	6.6×10^{21}
XO10	AS-17	V-20 Ti	Tensile	13	Argon-helium	500	7.2×10^{21}
XO10	AS-18	V-20 Ti	Tensile	13	Argon-helium	500	6.3×10^{21}
XO10	AS-19	V-20 Ti	Tensile	13	Argon-helium	500	6.6×10^{21}
XO10	AS-20	V-20 Ti	Tensile	13	Argon-helium	500	7.3×10^{21}
XO10	AS-21	V-20 Ti	Tensile	13	Argon-helium	500	8.7×10^{21}
XO10	AS-22	Hastelloy-X	Tensile	13	Argon-helium	500	7.6×10^{21}
XO10	AS-23	304 SS	Tensile	13	Argon-helium	500	8.7×10^{21}
XO10	AS-24	304 SS	Tensile	13	Argon-helium	500	7.3×10^{21}
XO10	AS-25	304 SS	Tensile	13	Argon-helium	500	7.0×10^{21}
XO10	AS-26	304 SS	Tensile	15	Argon-helium	500	7.1×10^{21}
XO13	AS-34	Hastelloy-X	Tensile	9	Sodium	650	2.8×10^{21}
XO13	AS-35	V-20 Ti	Tensile	9	Sodium	650	2.6×10^{21}
XO13	AS-36	V-20 Ti	Tensile	9	Sodium	650	2.5×10^{21}
XO13	AS-37	Hastelloy-X	Tensile	9	Sodium	650	2.8×10^{21}
XO13	AS-38	V-20 Ti	Tensile	9	Sodium	650	2.9×10^{21}
XO13	AS-39	V-20 Ti	Tensile	9	Sodium	650	2.8×10^{21}
XO13	AS-40	V-20 Ti	Tensile	9	Sodium	650	2.9×10^{21}
XO13	AS-41	V-20 Ti	Tensile	9	Sodium	650	2.6×10^{21}
XO13	AS-42	V-15 Ti-7.5 Cr	Tensile	9	Sodium	650	2.6×10^{21}
XO13	AS-43	V-15 Ti-7.5 Cr	Tensile	9	Sodium	650	2.7×10^{21}
XO13	AS-44	V-15 Ti-7.5 Cr	Tensile	9	Sodium	650	2.7×10^{21}
XO13	AS-45	V-15 Ti-7.5 Cr	Tensile	9	Sodium	650	2.6×10^{21}
XO13	AS-46	Hastelloy-X	Tensile	9	Sodium	650	2.9×10^{21}
XO13	AS-47	304 SS	Tensile	9	Sodium	650	3.0×10^{21}
XO13	AS-48	304 SS	Tensile	9	Sodium	650	2.9×10^{21}
XO13	AS-49	304 SS	Tensile	9	Sodium	650	2.9×10^{21}
XO13	AS-54	V-15 Ti-7.5 Cr	Tensile	9	Sodium	650	2.7×10^{21}
XO13	AS-55	V-15 Ti-7.5 Cr	Tensile	9	Sodium	650	2.8×10^{21}

D. Techniques for Fabrication and Testing

1. Ultrasonic Instrument and Transducer Development

Three ultrasonic transducer probes were fabricated this month. Two probes have lead zirconate-titanate elements from Gulton Industries (Type HDT-31), and Fiberglas-epoxy backings, one 1.27 cm long and one 2.22 cm long with a 30° cone at one end. The other probe has Clevite's PZT-4 type of lead zirconate-titanate. The probe has a 2.22-cm-long nickel backing (-500 mesh, 65.5% dense) with a 30° cone at one end. Evaluation of these probes and of the HDT-31 material is in progress.

Samples of sintered tungsten of various densities have been ordered to be evaluated for use as a backing member for ceramic transducer probes.

2. Neutron Image-intensification System

Following a preliminary television test of the gamma control amplifier with a visual test chart, the circuit was installed as part of the neutron television system. Tests with the neutron image of a plastic stepwedge indicated that the gamma control unit did extend the range of the neutron presentation. Without the gamma amplifier, only four steps on the stepwedge could be observed; with the gamma amplifier five steps could easily be observed. The gamma control unit has now been installed as part of the neutron television system.

A check on the light yield from the output phosphor of the neutron image-intensifier tube (with a 15-cm-dia target tube) has been made. After three months of use and an estimated 50 hr of neutron irradiation, the output phosphor brightness was still in excess of 100 ft-Lamberts for a tube acceleration voltage of 28 kV and an incident thermal neutron intensity of 2×10^7 n/cm^2-sec. The decrease in light yield of the intensifier tube, if any, was estimated to be less than 2%.

An experiment to determine the usefulness of the neutron television system for the detection of bubble patterns in water was performed. A water column width of 2.5 mm was used; metal shielding as thick as 1.9 cm of aluminum and 0.31 cm of steel was placed in the neutron imaging beam. The metal filters made essentially no difference in the excellent neutron image contrast of the water-bubble object, as observed in the television presentation. Motion and bubble patterns could easily be followed.

A similar experiment with the same object was conducted with an X-ray television system. The contrast was much less. The bubble patterns could be observed when no metal filter was used; the image became increasingly difficult to observe as aluminum and steel filters were added.

These experiments were performed because of our interest in possible application of the neutron television technique in fluid-flow investigations, and because of the expressed interest of R. A. Moss of Princeton University. The object used in the tests was meant to simulate a water fluid heat pipe.[12] Devices such as this are being studied at Princeton in order to optimize the heat transfer characteristics. As a result of the Argonne tests, a neutron test facility will be set up at the IRL Reactor at Princeton.

---

[12]Cotter, T. P., Theory of Heat Pipes, LA-3246 (Feb. 23, 1965).

3. Thermal Conductivity of Irradiated Fuel

The flash method of determining thermal diffusivity and thermal conductivity is being utilized to measure the thermal properties of AARR fuel plates. Measurements with the unirradiated material are made from ambient temperatures up to 800°C with intermediate measurements at 100°C increments. The 20 unirradiated samples include:

(a) Five samples from BMI sample plate No. 50.
(b) Five samples from Martin Company sample plate No. 48.
(c) Five samples from Sylcor full length plate No. 4.
(d) Five samples from BMI full length plate No. 57.

Measurements have been completed on the first 15 specimens.

E. Engineering Properties of Reactor Materials

1. High-temperature Mechanical Properties

The minimum strain rate versus stress for V-15 w/o Ti-7.5 w/o Cr tested at 650°C is plotted on semilogarithmic, log-log, and log-log hyperbolic sine coordinates in Fig. 6 for material vacuum annealed one hour at 900°C. For most metals the semilogarithmic plot best describes creep data at high stress levels (where $\beta\sigma > 3$) and the log-log plot, where σ^n is the stress function, best describes creep data at low stress levels. This would correspond to stresses of ≤ 15 kg mm^{-2} for the V-15 w/o Ti-7.5 w/o Cr alloy. The hyperbolic sine function has been suggested by Garofalo[13] to describe creep behavior over a large range of stress levels. Although all of the points in Fig. 6 cannot be fitted to a single straight line by any one of the three plotting methods, all three plots can be separated into two straight-line segments.

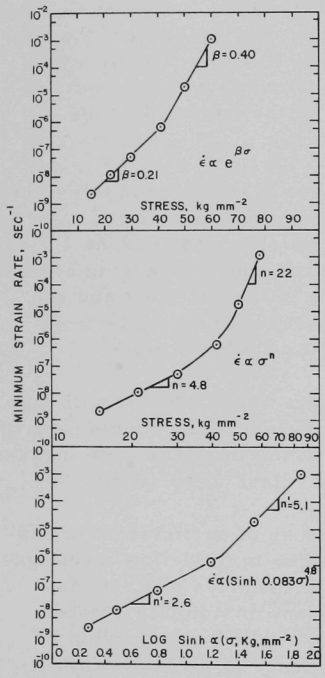

Fig. 6. Effect of Stress on the Minimum Creep Rate of V-15 w/o Ti-7.5 w/o Cr Annealed at 900°C for One hour and Tested at 650°C in $<1 \times 10^{-6}$ Torr

A change in slope of a minimum strain rate-stress plot may result from a change in rate-controlling mechanism. This minimum strain rate is plotted versus reciprocal temperature in Fig. 7 for a high stress level (60 kg mm^{-2}) corresponding to the region of

[13] Garofalo, F., Trans. AIME, 227, 351 (1953).

greater stress sensitivity and for a lower stress level (30 kg mn^{-2}) corresponding to the region of lower stress sensitivity to determine if the regions are associated with different activation energies. The activation energies are different by 15%. Further testing will be necessary to determine if this difference resulted from experimental scatter or is significant.

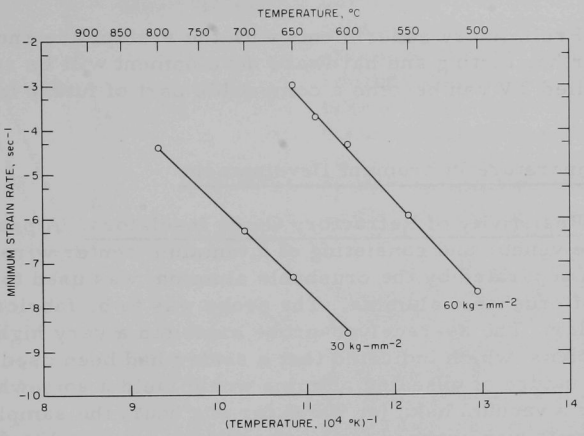

Fig. 7. Temperature Dependence of the Minimum Strain Rate of U-15 w/o Ti-7.5 w/o Cr Annealed at One hour at 900°C and Tested at 650°C

F. Engineering Development

1. Development of Master-Slave Manipulator System

a. Electric Master-Slave Manipulator, Mark E4A. The servo stability of the Mark-E4A manipulator was inadequate (see Progress Report for May 1966, ANL-7219, pp. 49-50). After considerable testing, several system changes are being incorporated that will increase the stability by at least a factor of two. This will make the E4A slightly more stable than the Model E3.

In the original system, the main limiting factor on stability was found to be the slow speed of the master motors relative to the slave motors. When the speed ratio of master motor to slave motor was increased from 0.4 to 0.6, the servo gain in the tachometer loop could be increased over 50%.

Other changes that give significant improvement are increasing the tachometer excitation (which improves the tachometer signal-to-noise ratio) and broadening the amplifier-frequency bandwidth to reduce phase shift of the tachometer sideband frequencies.

b. Head-controlled TV for Manipulator Systems, Mark TV2. This new experimental television system is now assembled and being tested with electric master-slave manipulators to evaluate the usefulness and practicality of head-controlled TV for future manipulator systems. In this system the camera and monitor are slaved to follow a manipulator operator's head in five motions.

Preliminary experiments with the system are encouraging. However, further testing and hardware development will be required before head-controlled TV can become a compatible part of future manipulator systems.

2. High-temperature Instrument Development

a. Resistivity of Refractory Oxide Insulators. A probe, constructed by an outside vendor and consisting of a tantalum center wire and tantalum outer sheath separated by the crushable alumina, was used to measure the resistivity of crushable alumina. The probe was to be fabricated without the use of a sealer. The as-received-probe exhibited a very high resistance, 4×10^5 megohms, which indicated that a sealer had been used, since the hygroscopic nature of unsealed alumina would yield a somewhat lower resistance. After a vacuum bake (at 900°C for one hour) the sample resistivity, when the sample was exposed to the atmosphere, dropped to 5×10^2 megohms. This indicated that the sealer was now largely removed. The fact that some sealer may have remained in the sample raises some doubt about the purity of the alumina, which was to be better than 99.6%.

A difference in the apparent resistivities of crushable and vitrified alumina is to be expected because of the different contact area between the electrodes and the insulation. The crushable type of insulation produces the greatest ratio of electrode-to-insulation contact area and is expected to exhibit the lower apparent resistivity. The vitrified type of insulator is slip-fit over the electrodes and will produce point or line contacts and, consequently, higher resistivity values.

This expected difference in resistivity was found when the resistivity of a crushable alumina sample was measured. The results are shown in Fig. 8 and are compared with previously reported data. As the sample temperature was increased to 1900°C, the resistivity values were found to be low. The sample was kept at 1900°C for one hour, during which time the alumina presumably vitrified. The resistivity values of this sample, as the temperature was slowly decreased (to avoid "frozen-in" defects--see Progress Report for March 1966, ANL-7193, p. 55) were then found to be representative of vitrified alumina.

The results of this test are significant for two reasons: (1) the test verified that crushable insulators exhibit a lower resistivity than

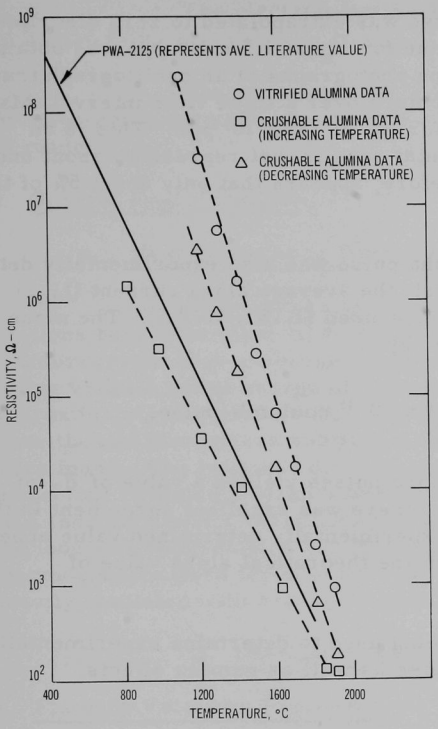

Fig. 8. Resistivity of Alumina

vitrified insulators; (2) the test demonstrated that a crushable insulator will vitrify at temperatures near the melting point. This means that if a thermocouple is to be used at temperatures near the melting point of the insulator, it does not matter whether vitrified or crushable insulators are used during construction since, after a short time at high temperatures, a vitrified insulator results in either case. The choice between the two types of insulators will be dictated by manufacturing convenience.

b. Wide-range Neutron-flux Monitoring. The lower limit of neutron detection for the mean current and mean-square-voltage portions of the wide-range neutron-monitoring system previously described (see Progress Report for March 1966, ANL-7193, pp. 56-7) is determined by the unwanted pulses caused by either the alpha particles produced by the natural radioactive decay of the fissionable coating itself or by the residual gamma flux.

To be able to predict accurately the output signal caused by these unwanted pulses, the total number of pulses produced and the mean and mean-square charge per pulse for each radiation must be determined.

The number of alpha particles produced by natural disintegration of an isotope of half-life T years is about $5.6 \times 10^{10}/T$ pulses/sec-mg for a material of atomic weight near 235. For pure U^{235}, an alpha pulse rate of 78.5 pulses/sec/milligram (pps/mg) is expected; for pure U^{238}, 12.3 pps/mg; for U^{234} 2.27×10^5 pps/mg. The fission counter used had 1840 mg of total uranium with 1720 mg of U^{235}. The contribution due to the U^{235} is, therefore, 1.35×10^5 pps. The remaining 120 mg is composed of U^{234} and U^{238} in some unknown proportion. If it is assumed that 10% of the remaining uranium is U^{234}, the total pulse rate due to alpha particles is 2.86×10^6 pps = $\overline{N}_\alpha$.

The total number of alpha pulses produced by the fission chamber coating was experimentally verified in two different ways. First, the

measured integral bias response curve was extrapolated to zero discriminator voltage. By this method, a value for $\bar{N}_\alpha$ of 1.5×10^6 pps was obtained. The second method consisted of taking photographs of an oscillograph trace of the alpha pulses and counting the pulses over a finite time interval. Many such measurements yielded a value for $\bar{N}_\alpha$ of 1.3×10^6 pps. This is an excellent agreement of the experimental results, but represents about one-half of the calculated value. It, therefore, appears that only about 5% of the remaining uranium was U^{234}.

The mean charge per alpha pulse was also experimentally determined by two different methods. First, the average alpha current ($I_{dc\alpha}$) produced by the fission counter was measured (1.18×10^{-8} A). The mean charge per pulse was then determined by:

$$\bar{q}_\alpha = \frac{I_{dc\alpha}}{\bar{N}_\alpha} = \frac{1.18 \times 10^{-8}}{1.3 \times 10^6} = 9.1 \times 10^{-15} \text{ coulomb/pulse.}$$

The photographs of the alpha pulses yielded a value of $\bar{q}_\alpha$ of 1.1×10^{-14} coulomb per pulse. Again, there was excellent agreement in the experimental results, but again the experimentally determined value appears to differ by about a factor of two from the theoretical alpha value of 2×10^{-14} coulomb per pulse.

Similar techniques are being used to determine experimentally, the mean-square charge per alpha pulse as well as gamma effects.

3. Boiling Liquid-metal Technology

a. Niobium-1% Zirconium Loop. Repairs to the roughing pump seals (see Progress Report for June 1966, ANL-7230, p. 41) are complete and the vacuum chamber has been returned to operation.

The Nb-1% Zr loop was filled, and sodium has been circulated at velocities up to 15 ft/sec at 400°F and a maximum pressure of 200 psia.

b. Heater Experiments

(i) Electron-bombardment Heater Experiment. Approximately 375 hr of testing with the 0.030-in.-dia thoriated-tungsten filament have been achieved. Heat fluxes exceeding 350,000 Btu/hr-ft^2 have been supplied to the anode during both steady-state and transient testing with peak sodium temperatures to 1400°F. This includes an emission current range to 5.2 A and a cathode-to-anode voltage of 7700 V. These tests are yielding information pertinent to the design of a reliable high-temperature, high-heat-flux electron-bombardment heater for use in the Nb-1% Zr loop.

The electron-bombardment heater design study was made by Eimac Corp.

The recommended designs are being reviewed and a final decision concerning the appropriate heater for the NB-1% Zr loop will be made.

4. General Heat Transfer

a. Heat Transfer in Double-pipe Heat Exchangers

(i) Countercurrent Turbulent Liquid-metal Flow. Final preparations have been made to start the experimental part of the liquid-metal, countercurrent heat-exchanger program. The loop was cleaned prior to filling with an initial charge of mercury. The mercury was circulated for approximately two weeks while the loop was checked for leaks. During this time, the emf flow meters and pressure transducer were calibrated. Two leaks were found. The loop was drained, dismantled, and the leaks were repaired. Inspection revealed a definite wetting of the copper wall in the test section, so a thermal contact resistance is not anticipated. With the leaks repaired, the loop was reassembled and filled with a fresh charge of mercury. Shielded thermocouples were taped to the test section. The entire loop was then heavily insulated with Fiberglas insulation.

G. Chemistry and Chemical Separations

1. Fluoride Volatility Processes

a. Recovery of Uranium and Plutonium from Low-enrichment Fuels: Laboratory Support Work

(i) Fluorination of UO_2-PuO_2-fission Product Pellets. Development studies are being performed in a 2-in.-dia fluid-bed reactor to determine optimum conditions for fluorinating UO_2-PuO_2 pellets containing fission products. Recent experiments have involved the use of BrF_5 as a selective fluorinating agent for conversion of uranium oxides in uranium-plutonium mixtures to UF_6. In this reaction, plutonium is converted to nonvolatile PuF_4. Recovery of plutonium as volatile PuF_6 is effected in a subsequent step by reaction of PuF_4 with fluorine at temperatures of 300 to 550°C. A recent experiment (Purse-8) completed a series of runs to determine the effect of the temperature of the BrF_5 fluorination step upon plutonium retention in the final alumina bed. In previous experiments of this series, BrF_5 fluorination temperatures of 200°C (see Progress Report for April 1966, ANL-7204, p. 63) and 300°C (see Progress Report for February 1966, ANL-7176, p. 65) were evaluated. In the recent experiment, the BrF_5 fluorination step was carried out at 400°C. The charge to the reactor

consisted of 650 g of pellets and 1100 g of alumina containing 0.6 g cesium fluoride. The fluorination sequence for the recovery of uranium and plutonium was carried out as follows: oxidation of the pellets for 4 hr at 450°C with 20 v/o oxygen, fluorination with 10 v/o BrF_5 in nitrogen for 1.7 hr at 400°C, followed by recycle-fluorination with 90 v/o fluorine for 3 hr at 300°C, 5 hr while the temperature of the reactor was increased from 300 to 550°C at 10°C/12 min, and 3 hr at 550°C.

The concentration of both uranium and plutonium in the alumina bed after recycle-fluorination was 0.012 w/o, which is slightly higher than that obtained at 200°C (0.003 w/o uranium and 0.009 w/o plutonium) and at 300°C (0.007 w/o uranium and 0.007 w/o plutonium). It appears that the BrF_5 fluorination temperature does affect slightly the extent of plutonium removal during recycle fluorination and, on the basis of these data, 300°C is the best temperature for conducting the BrF_5 fluorination step.

(ii) Neptunium Fluoride Chemistry. Laboratory-scale studies of the reaction of NpF_4 with BrF_5 are being carried out to determine the behavior of neptunium when oxidized nuclear fuel is contacted with BrF_5. A series of experiments have been carried out in a boat reactor to determine the rate of reaction at 300, 325, 350, and 450°C using a gaseous mixture containing 33 v/o BrF_5 in nitrogen. At temperatures between 300 and 350°C, the rate of reaction can be described by a diminishing-sphere model. An activation energy of 26 kcal/mole was calculated from the rate data over this temperature range. The rate constants calculated at 300, 325, and 350°C were significantly lower (by a factor of 10^{-2}) than those measured in the same temperature range for the UF_4-BrF_5 reaction. The reaction between NpF_4 and BrF_5 at 400°C does not appear to conform wholly to the diminishing-sphere model and further experiments are required before a suitable model can be developed to describe the reaction.

b. Recovery of Uranium and Plutonium from Low-enrichment Fuels: Engineering Work

(i) Engineering-scale Alpha Facility. The major objectives of experiments conducted in the engineering-scale alpha facility are to investigate the possible difficulties in handling PuF_6 on an engineering scale and to determine the feasibility of fluoride volatility flowsheets. Later experiments may be performed with low levels of fission-product activity. Current work in the facility involves the recovery of the residual amounts of plutonium deposited in process-equipment lines and vessels during previous fluorination experiments as a result of chemical reaction, thermal decomposition, or alpha decomposition. During the recovery operation, fluorine is recycled through the equipment at temperatures of 275 to 400°C. The PuF_6 produced by reaction of fluorine with the plutonium deposits is

sorbed on sodium fluoride pellets at 125°C. With additional data pending, results obtained thus far indicate that less than 15 g of plutonium (from an input of 116 g) have not yet been accounted for; the plutonium material balance throughout the fluorination experiments may be significantly improved as a result of complete analyses, currently being made, of the plutonium content of the feed material.

Plutonium hexafluoride is readily sorbed on a bed of sodium fluoride. At a bed temperature of about 125°C, the sorption efficiency was high; >95% of the plutonium hexafluoride was sorbed in the inlet portion of the bed, whereas at lower bed temperatures (about 50°C), the sorption efficiency was slightly lower.

A series of experiments are under way to demonstrate the transfer of PuF_6 in process equipment. These experiments will involve such operations as the fluorination of PuF_4 in the fluid-bed reactor and the transfer of the PuF_6 from the reactor to a bed of sodium fluoride pellets, and the transfer of PuF_6 from one vessel to another. The experiment involving the fluorination of PuF_4 (Run Pu-6) has been completed. In this experiment, approximately 134 g of PuF_4 in a fluidized bed of alumina (6750 g of -48 +100 mesh alumina) were fluorinated with 100 v/o fluorine at temperatures from 200 to 550°C. Near the end of the run, the temperature of the wall of the filter chamber was increased from 125 to 300°C to fluorinate any plutonium deposited within the filter chamber. The total fluorination time was 49.5 hr. The PuF_6 product was collected on a bed of sodium fluoride. Preliminary analyses of the final alumina-bed material indicate that >99.9% of the plutonium charged to the fluid-bed reactor was removed from the bed during fluorination.

2. Closed Cycle Process

a. Thorium Distribution Data. The chemistry of thorium in liquid metal-molten salt systems is of interest in the development of recovery processes for thorium-based reactor fuels. In recent work, thorium distribution coefficients were determined for the following systems: (1) between 50 m/o $MgCl_2$-30 m/o NaCl-20 m/o KCl and Zn-10 w/o Mg alloy, and (2) between the same ternary salt and Cu-8 w/o Mg alloy. In both systems, thorium distributed strongly in favor of the metal phase. At 800°C, the distribution coefficients (w/o thorium in salt/w/o thorium in alloy) were $\sim 10^{-4}$ in the case of the zinc-magnesium alloy and $\sim 10^{-3}$ in the case of the copper-magnesium alloy.

III. ADVANCED SYSTEMS RESEARCH AND DEVELOPMENT

A. Argonne Advanced Research Reactor (AARR)

1. Physics Experiments and Analyses

a. Enlarged ITC. The enlargement of the internal thermal column (ITC) was made possible by removing 7 plates in each of the 6 fuel assemblies bordering on the ITC (see Progress Report for June 1966, ANL-7230, pp. 48-9); the result is designated to be a "1173/1566" core loading. The loss in reactivity is estimated to have been about 2½%. The resulting reactor was subcritical by ~0.3%, as inferred from the void introduced in the ITC to take the reactor to delayed criticality. To compensate for this reactivity loss, an additional 219 B-SS strips have been removed and replaced with stainless steel, leading to a "1173/1347" loading. Criticality was attained with two control blades fully inserted, and a third blade partially inserted. Local calibration checks give preliminary indications of increases in control blade worth: ~12% for an in-core blade, and a percentage increase of ~27% for a peripheral control blade. The available excess reactivity in the modified reactor, therefore, is estimated to be ~3½%.

In the enlarged ITC, experiments have been performed with full-length beryllium parallelopipeds replacing water at the axis of the ITC. Introduction of a 1 x 1-in. beryllium block increased reactivity by 0.26%. A 2 x 2-in. block was worth 0.94%. Additional experiments will be performed with rings of beryllium replacing water at the outer boundary of the ITC.

A set of ITC-voiding experiments has been completed for the oversized ITC. Preliminary results indicate that the maximum positive reactivity effect of the full-length fractional voidings of the ITC would occur in the vicinity of 65-70% average void in the ITC. This compares with a peak reactivity gain at 50-55% void, in the small ITC.

b. Theoretical Studies. In the majority of the computations performed for the various loadings of the Criticality Facility and for the design reference for AARR, a uniform, equivalent bare-region height of 60 cm was assumed. This corresponds to a total axial reflector savings of 14.3 cm. Figure 9 shows a summary of the effects on reactivity if this bare height is changed uniformly in all radial regions of the PSAR-reference reactor. The case of zero reactivity change is the reference 60-cm height. A variation of +4 cm (-4 cm) yields a reactivity variation of +1.2% (-1.5%). The original choice of a 60-cm equivalent bare height was based upon 2-dimensional computations. Additional 2-dimensional computations are being performed to study the higher-order effects on reactivity due to changes in the axial reflector savings for cases of large perturbations of

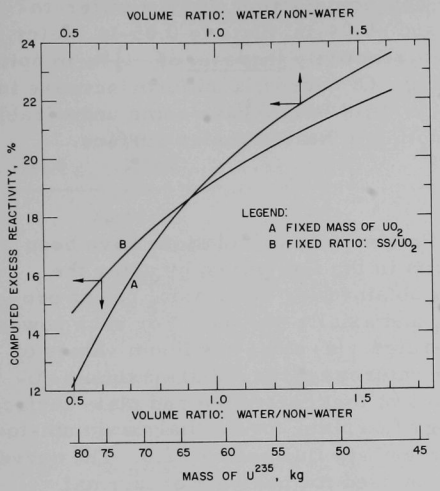

Fig. 9. Available Excess Reactivity for Clean Cold AARR, without Grading of Fuel Loading, vs. Water Content of Reactor Fuel Zone

the Internal Thermal Column. Examples of such perturbations are: (i) massive fractional voidings, and (ii) inserts containing significant volumes of samples and diluents.

The choices of the thicknesses of fuel plates (0.04 in.) and coolant channels (0.04 in.) in the design reference AARR core represent a compromise between desired reactor physics features and cooling requirements. In Fig. 10 are summarized the effects on available excess reactivity if the overall water content of the fuel zone were altered. Each of the two curves corresponds to a change in the volume fraction of water with a compensating change in the volume fraction of "metal" (nonwater). In each case, the fuel-zone materials were assumed to be effectively homogeneously distributed.

For one set of computations, the ratio of stainless steel to UO_2 was held constant (approximately), representing, for example, a change in coolant-channel thickness. For the other computations, the total UO_2 content of the reactor core was held constant. This latter case represents, for example: a change in the thickness of the fuel-plate cladding, or changes in the thickness of the fuel-plate matrix and the size of the coolant channel, keeping invariant the total mass of UO_2. The "reference" reactor of these analyses is the PSAR-reference system except that there was no spatial grading of the fuel loading.

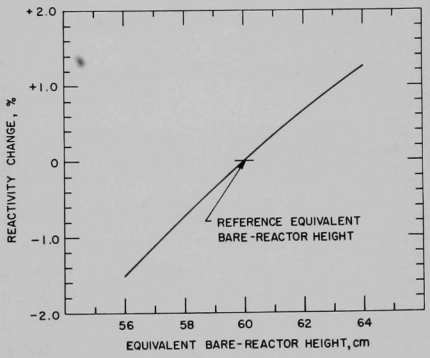

Fig. 10. The Effect of Equivalent Bare-reactor Height on Reactivity (AARR PSAR Reference Reactor)

An increase in the water content of the fuel zone results in a reactivity gain, even if the UO_2 content was decreased. To illustrate, increasing the volume ratio of water to nonwater from 0.9 (+) to 1.0 would yield a reactivity increase of: ~0.7% for the case of a decreased UO_2 content, and ~1.0% for the case of fixed UO_2 content. This change corresponds approximately to removing 5% of the nonwater content of the fuel zone and replacing it with water.

A change in the fuel-plate cell composition, from a water-to-metal ratio of 0.04-in. water channel and ~0.04-in. plate to 0.05-in. water channel and 0.04-in. plate, would yield a reactivity increase of $1\frac{1}{2}$%, in spite of a decrease of ~$12\frac{1}{2}$% in the fuel loading. Of course, a uniform increase in coolant-channel thickness, from 40 to 50 mils, would have some undesirable ramifications, for example, a 12% reduction in heat-transfer surface.

2. Fuel and Core Development

a. Heat Transfer Analysis. Preliminary calculations have been made to determine temperature patterns in the fuel plates by using the computer code STDY-3. Results were obtained for three axial power profiles: axially uniform, axially peaked, and axially skewed. For each power profile the following curves were generated: (a) axial maximum values of fuel centerline and plate surface temperatures versus radial maximum-to-average power density; (b) axial profiles of fuel centerline and plate surface temperatures versus heated length along a fuel plate, for a radial maximum-to-average heat flux ratio of 2.0. The curves will be used for analysis of thermal stresses.

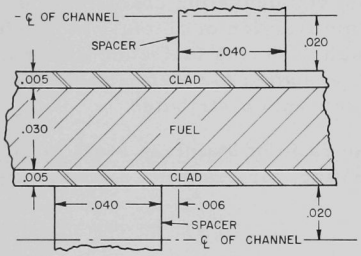

Fig. 11. Fuel Plate-Space Configuration

An investigation was made to determine the effects of reduced heat transfer in the corner regions and degree of bonding of the spacer for the fuel plate-spacer configuration shown in Fig. 11. The study was undertaken as part of a general evaluation of the effect of fuel underneath the spacers. The cross section of a fuel plate, cladding, and spacers, divided into a mesh of nodes, was run as a two-dimensional case with the computer code THTB. Table XIV summarizes the cases studied. The results are being analyzed.

Analysis has shown that for case 1, insulated within 3 mils of the corners, the following applies to 100-MW operation: (a) an inlet pressure of 708 psia is required to suppress local boiling with a 45-ft/sec coolant velocity and fuel under the spacer (this is contrasted with only 275 psi being required with no fuel under the spacer); (b) the fuel-plate centerline temperature was calculated to be 65°F greater (707°F) under the spacers than at some distance from the spacers (642°F). This can be compared with the situation where the corners are uninsulated, which indicated a temperature difference of 35°F greater (677°F) than the unperturbed maximum of 642°F.

TABLE XIV. Summary of Fuel Plate-Spacer Results

Case	Spacer Bond	Heat Transfer Coefficient in Corners	Temp (°F)		Ratio of Hot-spot Heat Flux to Unperturbed Heat Flux
			Surface	Internal	
1	Bonded both sides	Zero	490	707	1.47
2	Nonbond of 0.030 in. one side	Zero	533	790	1.68
3	Nonbond of 0.03 in. both sides	Zero	547	802	1.77
4	Nonbond of 0.030 in. both sides	1/2 of full value	492	783	1.56
5	Nonbond of 0.030 in. one side	Full value	448	762	1.47

Since the AARR has a specified 750-psia inlet pressure no local boiling would occur at 100 MW. The ratio of the hot spot to unperturbed heat flux listed in Table XIV must be evaluated. Indications from the heat transfer tests are that high local values are permissible. An evaluation of this situation for the overall design will be made.

The increased temperatures in the fuel with good bonding are not excessive in terms of allowable temperature for the expected number of fissions/cc. Severe nonbonds, such as in case 3, require more detailed evaluation.

b. Steady-state Tests. In the steady-state heat transfer program, the effect of channel spacing, flow, inlet water temperature, pressure and power upon pressure differential along the channel, void distribution, and critical heat flux are measured with electrically heated, rectangular test sections that simulate the flat-plate geometrical arrangement of the AARR core.

A test section has been assembled by a new procedure to reduce dimensional variations in the flow channel. The average channel spacing after assembly and hydrostatic testing was 0.051 in., with a maximum deviation of ±0.001 in. Test measurements were made with an eddy current probe with the section in a no-flow, no-pressure condition. The section was then installed in the loop, and instruments were attached and calibrated.

Pressure drop from channel inlet to outlet was recorded for various operating ranges. Calculations based on these numbers showed the average channel spacing opened up to 0.052 in. with pressure, flow, and power approximately equivalent to an average channel in AARR at 100-MW operation.

Heat balances for the new section showed ~2% heat loss through the back system.

Final adjustment on the γ-ray void measurement will complete shakedown tests on this section.

c. Shutdown Emergency Cooling. The shutdown-emergency cooling tests are intended to determine the allowable time intervals following shutdown for specific operations such as core unloading. Such tests will furnish guidance of the reactor design effort in this regard.

Burnout limits will be determined at low flow rates and power levels during natural circulation and during flow reversal from downflow to upflow prior to the establishment of natural circulation after shutdown. Specific safety tests concerning fuel-handling problems will be studied also.

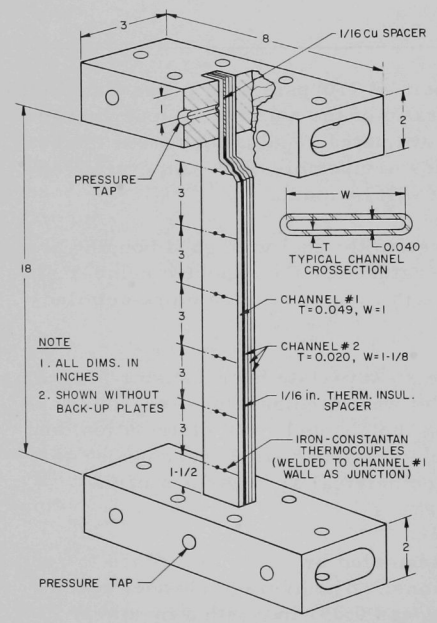

Fig. 12. Four-channel Test Section

Construction of the Shutdown-Emergency Cooling Loop has been completed. The loop, a recirculating closed system, with forced-circulation downflow or natural-circulation upflow through the four-channel heated test section shown in Fig. 12, has operated satisfactorily. Pertinent data are shown in Table XV.

Tests have been conducted in the loop with the test section. The operational procedure is to begin forced-circulation downflow at test-section velocities of 7-8 ft/sec and to set desired values of system pressure and test-section power at the fixed inlet temperature of 135°F. With the system thus stabilized, pump power is cut off and the flow reverses to natural-circulation upflow. Continuous recordings of inlet and exit coolant temperature, flow, power, and system pressure are made during the flow reversal and natural-circulation stabilization process.

Hot-channel outside wall temperatures are recorded at intervals of 5 sec/thermocouple; a complete profile is obtained every 30 sec. When burnout conditions are anticipated, the uppermost wall thermocouple ($1\frac{1}{2}$ in. from the end of the heated length) is switched to a fast-response (1/4-sec) continuous recorder to serve as a visual burnout alarm. When stabilized (but not necessarily stable) natural circulation has been established, the pump is cut in to re-establish forced-circulation downflow, and the test-section power is increased to the next desired level. The above procedure is then repeated through increasing power levels until a defined burnout condition is achieved. No physical burnout has yet occurred.

TABLE XV. Loop and Test-section Data

System pressure	15-1000 psig
Pump	30 gpm @ 60 psi head
AC power supply	40 kW
Ratio of hot channel to avg channel average heat flux	2.5
Ratio of max peripheral to average heat flux in hot channel	2.2
Axial heat flux distribution	Uniform

A total of 37 flow-reversal data points has been run at a system pressure of 750 psi, 135°F inlet coolant temperature, and forced-circulation velocity of 7-8 ft/sec. An arbitrarily defined burnout condition (surface temperature 300°F greater than nucleate-boiling surface temperature) was encountered at a hot-channel average heat flux of 193,000 B/hr-ft^2. Acceptable values of measured maximum surface temperature (760°F and natural-circulation flow stability) were measured at hot-channel average heat fluxes up to 180,000 B/hr-ft^2. This corresponds to a reactor power level of approximately 9 MW.

Analysis of the low-pressure (15-psig) data obtained from the loop shows acceptable natural-circulation flow stability at hot-channel average heat fluxes up to 35,000 B/hr-ft^2. The corresponding reactor power level is approximately 1.75 MW. At the same minimum pressure, increasing natural-circulation flow instability was encountered at hot-channel average heat fluxes up to 70,000 B/hr-ft^2. Despite the extreme instability, including downward percolation from the test section, tentative conclusions that can be drawn from the existing data are:

(i) Safe flow reversal can be accomplished at significantly greater power levels at reactor operation pressure of 750 psi, rather than after depressurization, has been validated by test data.

(ii) Natural-circulation instability appears to be more of a limitation on power than flow-reversal thermal transients.

(iii) Initiation of core-removal operations seems to be limited primarily by natural-circulation instability levels considered permissible during the removal, transport, and storage of the reactor core.

(iv) Design and installation of a forced-circulation, flow-reversal system appears unnecessary because of the unexpectedly high power levels at which natural-circulation flow reversal may occur.

d. Fuel Hydraulic Tests. Electron-beam welding of abutting machined center ribs of shaped test pieces made of Type 304 and 430 stainless steel indicates that distortion and clamping during welding a center spacer rib are major problems because of the channel tolerances desired. Therefore several alternative approaches to the attachment problem are being investigated. Forming of spacer ribs on stainless steel sheet is being attempted by a chemical milling technique as an alternative to production of ribs on simulated fuel plates by machining.

e. Fuel Quality Control and Inspection.

(i) Plate-loading Homogenity. All equipment has been received and assembled by IITRI. Preliminary tests indicate the system is operative; however, the exact capabilities and optimization of the system remain to be accomplished.

(ii) Channel-gap Measurement. Preliminary frequency analysis of strain-gauge probe data indicates that most of the data is in the 0-20 cps range and considerable 60- to 120-cps noise is in the signal. Additional development efforts to filter the signal and provide a reasonable signal and recording are being undertaken.

f. Fuel-assembly Development. Phases Ia and Ib of the Braze contract with Pyromet have been completed. Phase Ia consisted of a series of 24 experiments evaluating 3 braze alloys, a range of brazing temperatures (1825-2150°F), and braze-time duration (10 min at braze temp 2 hr hold at lower temp; 2 and 3 hr at braze temp). The results of the visual and metallographic examination of 5 plate sections and shear testing of 3 samples brazed under combinations of the above conditions indicates that acceptable and consistent braze results are obtained with use of GE-J8100 alloy, and that good joints and fillets are obtained at brazing temperatures ranging from 2075 to 2100°F for durations of from 2 to 3 hr. Samples tested in the most r producible mode for shear indicated loads in the range of 1900 to 2300 lb on ribs 0.040 in. wide by 0.375 in. long brazed to a backing plate.

Phase Ib consisted of brazing 6 dummy fuel elements by the present best method on a best-efforts basis. They were brazed with GE-J8100 alloy for 2 hr at 2135-2145°F. The elements have been received, and are to be inspected and evaluated for dimensional tolerances and for braze quality by nondestructive inspection techniques.

The first unit has been partially inspected. Dimensions across spacers (2.200 in. nominal) ranged from 2.200 to 2.211 in. However, the dimension across the plates (2.120 in. nominal) varied from 2.122 to 2.124 in. at the ends to 2.118 to 2.120 in. at the centers. Dimensions across flats (2.460 in. nominal) ranged from 2.464 to 2.486 in. This variation appears to be the result of excess braze material on these edges.

Several of the assemblies have areas of incomplete melting and brazing of portions of the external center and edge spacer wires on the plates. This was found to be caused by outgassing of the "stopoff"* material used on shims between the assemblies and the brazing fixture. Elimination of the stopoff on these shims eliminated this problem.

g. Control-rod Development. Hafnium has been received for the prototype rod. Zircaloy-2 material for a 6-in. control-rod follower is on order. Type 347 stainless steel to be used for the follower on the Eu_2O_3 rod has been sent out for rolling to 0.200-in. thickness.

h. Uranium Burnable Poison Fuels. The useful life of a reactor fuel element may be extended by adding a burnable poison to its structure, either as a discrete phase in the element or in intimate mixture with the fuel compound itself. Work is proceeding to incorporate boron into UO_2 to serve as a burnable poison. For use in this work two boron compounds, UB_2 and UB_{12}, have been prepared. The diboride of uranium was prepared by reacting UH_3 with B. The powdered materials were mixed, pressed, and reacted at 1450°C in vacuum. The UB_2 produced was essentially one phase with very weak reflections for TaB_2 (specimens were set on tantalum). Uranium dodecaboride was prepared by reducing UO_2 with boron. The mixed powders were pressed and reacted in flowing argon at 1480°C. The reacted material was predominantly UB_{12} with a_0 = 7.472Å and weak to moderate reflections for UB_4. Again there appeared to be some reaction with the tantalum on which the specimens were set during reaction, but no tantalum phase appeared in the X-ray pattern.

3. Component Development

a. Reactor Vessel. The preliminary study of the AARR pressure vessel containment potential has been completed. The purpose of the study

*A proprietary product of Wall Colmonoy Corp. (trade name "Green Stopoff") which prevents braze material from adhering to coated areas during the braze cycle.

is to find the magnitude of the nuclear excursion that the AARR pressure vessel is capable of containing without causing rupture of the vessel wall. Upper bounds in terms of pounds of TNT were estimated. The results of this study are summarized in the following:

(i) For the case of no water in the reactor pool and no loss of water from the vessel immediately prior to the accident, the TNT containment potential of AARR vessel is estimated to be 130 lb TNT, which is equivalent to 260 MW-sec.

(ii) If all of the vessel water was lost immediately prior to the accident, the containment potential would exceed 260 lb TNT (520 MW-sec). For portions of the vessel water lost, the potential would range between 130 and 260 lb TNT.

(iii) If all reactor pool water was retained, the inertia of the reactor pool would increase the containment potential of the vessel to more than 260 lb TNT (520 MW-sec).

(iv) For slow-release nuclear excursions, the energy absorption potential of the vessel wall increases by at least a factor of 3.

(v) The peak internal blast pressure resulting from the detonation of 130 lb TNT is about 1670 psia, which is far less than the static bursting pressure of the vessel. Hence, no further distortion of the vessel wall will be produced by the internal blast pressure.

(vi) Neither the shock wave nor the internal blast pressure from the detonation of 130 lb TNT is strong enough to cause the top head to act as a missile if high-strength bolts are used as the bolting material and all the bolts are in the tightened position.

b. Stress Analysis of Beam-tube Adapter. An analysis has been made of the stresses in the high-pressure portion of the beam-tube adapter in order to understand the effects of various loads and assembly procedures. The high-pressure portion of the beam-tube adapter lies between the vessel nozzle and the beam tube seal connection (see Progress Report for February 1966, ANL-7176, p. 83). The adapter is subjected to bending moments caused by: (i) the weight of internal shielding, (ii) restraint of the end of the adapter during thermal expansion of the reactor vessel and its support, and (iii) the reaction to the beam tube cantilevered from the adapter. Results for the following cases were calculated and are given in Table XVI.

I and IA. The adapter is fixed (without deflection) at its end by a support near the face of the biological shield. Internal shielding is installed and the vessel is heated.

TABLE XVI. Summary of Stress Calculations for Beam-tube Adapter

Case	Vessel Condition	Length of Adapter (in.)	End-deflection* (Vertical) (in.)	Reaction* at Support (lb)	Moment at Reduced Section (in.-lb)	Bend Stress at Reduced Sect. (psi)	Moment at Nozzle Face (in.-lb)
I	Cold	109	0	+3870	-27,300	550	-40,200
	Hot		-0.050	+2530	-168,600	3,400	-187,500
II	**		-0.144	0	-433,500	8,750	-463,900
III	Cold		-0.144	0	-433,500	8,750	-463,900
	Hot		-0.194	-1360	-576,500	11,600	-612,700
IV	Cold		+0.060	+5480	+141,400	2,850	+135,600
	Hot		+0.010	+4130	0	0	-11,700
I	Cold	89	0	+2280	-25,500	510	-35,200
	Hot		-0.050	-30	-219,300	4,430	-236,300
II	**		-0.049	0	-219,000	4,420	-239,000
III	Cold		-0.049	0	-219,000	4,420	-239,000
	Hot		-0.099	-2240	-409,100	8,250	-439,200
IV	Cold		+0.057	+4900	+196,900	3,890	+198,900
	Hot		+0.007	+2580	0	0	-8,400
IA	Cold	109	0	+4000	-13,900	280	-27,200
	Hot		-0.050	+1810	-243,400	4,910	-265,700
IIA	**		-0.091	0	-433,500	8,740	-463,900
IIIA	Cold		-0.091	0	-433,500	8,740	-463,900
	Hot		-0.141	-2170	-661,100	13,340	-701,300
IVA	Cold		+0.053	+6320	+229,500	4,620	+227,500
	Hot		+0.003	+4130	0	0	-11,800
IA	Cold	89	0	+2450	-11,000	223	-20,100
	Hot		-0.050	-1065	-359,000	7,250	-334,200
IIA	**		-0.035	0	-219,000	4,410	-239,000
IIIA	Cold		-0.035	0	-219,000	4,410	-239,000
	Hot		-0.085	-3525	-518,200	10,450	-554,000
IVA	Cold		+0.052	+6105	+299,200	6,040	+306,600
	Hot		+0.002	+2580	0	0	-8,400

*Support reactions and deflections are positive upwards, deflections measured from nozzle centerline.
**Loading independent of vessel temperature.

II and IIA. The adapter with internal shielding is cantilevered from the reactor vessel nozzle.

III and IIIA. The adapter is deflected by the weight of internal shielding, then fixed at the end in the deflected position, and the vessel heated (an undesirable procedure).

IV and IVA. The adapter is loaded with shielding, then cold sprung to counteract the shielding weight and thermal expansion to yield zero bending stress in the smallest section during hot operation.

Calculations were made for the adapter with and without its extension, giving total lengths of 109 and 89 in. In Cases I-IV unrestrained bending in tubular sections was assumed, and in Cases IA-IVA a tight-fitting shielding was assumed to restrain bending in the stepped tubular sections (i.e., the moment of inertia was taken to be that of a solid rather than the hollow section as assumed for Cases I-IV).

It was estimated that the portions of the reactor vessel and its support cylinder (thermal shield) which affect the location of the beam-tube nozzles would expand 0.050 in. vertically in going from the cold (assembly) to the hot operating condition. Internal shielding at an average density of 500 lb/ft^3 was assumed to fill the back end of the adapter. Since this

assumption does not represent a specific shielding design, the tabulated results should only be considered typical of what might actually occur.

An axially directed force of 58,000 lb due to pool and reactor pressure also acts on the adapter, creating a tensile stress of 2500 psi which is additive to the stress values at the reduced section given in Table XVI. Some small lateral bending loads which result from diametral thermal expansion of the vessel have not been tabulated. Reference to Table XVI shows that the stresses in the reduced section in all four cases are well within the design stress intensity value of 20,000 psi for stainless steel at this temperature.

c. Beam-tube Emergency and Shutdown Cooling. Some limiting-type calculations were made to estimate beam-tube temperatures after loss of flow with and without reactor scram. Although these situations cannot presently be rigorously examined, the following results were obtained through the use of simple analytical models which assume no transfer of heat from the local region under consideration:

(i) Conditions after loss of flow with reactor scram from 240MW

Time for beam-tube metal to reach 350°F	>10 min
Time for beam-tube metal to reach 500°F	>45 min
Time for coolant to reach saturation temp (511°F)	>79 min
Time to completely evaporate coolant locally	>167 min

(ii) Conditions after loss of flow, reactor at 240 MW without scram

Time for beam-tube metal to reach 500°F	>10 sec
Time to completely evaporate coolant locally	>81 sec
Rate of temperature rise of vapor "insulated" tube	~24°F/sec

The conclusions from this study are: i) that an uninterrupted pump power supply is not required for supplying coolant to remove decay heat from the beam tubes, and ii) that complete loss of flow to the beam tubes should initiate a reactor scram.

d. Material Compatibility and Corrosion. The final test in which a stainless steel specimen was subjected to a heat flux of 2×10^6 Btu/hr/ft^2 across its water-cooled interface (see Progress Report for May 1966, ANL-7219, pp. 73-74) was terminated after an uninterrupted 2000-hr test. The temperature of the specimen remained essentially constant during the test, indicating no significant buildup of corrosion products on the water-cooled surface. Visual examination of the specimen showed the surface to be coated with a thin, tarnish-like film. Sections of the specimen will be

metallographically investigated to determine, if possible, the thickness of the surface layer and whether localized attack of the stainless steel occurred.

The isothermal test with crevice and galvanically coupled specimens of aluminum, beryllium, and stainless steel was also terminated. The samples had been exposed to deionized water at 200°F for 3655 hr. Although the examination is incomplete, preliminary observations indicate no serious attack on any of the specimens.

The experimental portion of the corrosion test program is now complete. When the examination of the test specimens is finished, a report encompassing all of the result of this program will be prepared.

IV. NUCLEAR SAFETY

A. Reactor Kinetics

1. Irradiated Fast Reactor Oxide Fuel Pins

The four, stainless steel-clad, gas-bonded, half length EBR-II size previously irradiated oxide pins that were exposed in TREAT (see Progress Report for June 1966, ANL-7230, p. 62) have been returned to the Illinois site for inspection in the hot laboratory facilities.

Transient temperatures were calculated from the experimental data and the ARGUS heat transfer code.[14] Since central voids were observed in the control specimens, the original fuel density of the pins was corrected to allow for the radial migration which produced the voids. Sample burnup values for the calculations were obtained by radiochemical analyses of exposed monitor wires, corrected for the difference between the flux at the monitor-wire position and the average fuel flux. Direct measurements of burnup were also obtained from mass-spectrometer analyses of four control specimens: the mass-spectrometric values averaged 12% less than those obtained from the monitor-wire measurements. The energy inputs used in the calculations were based on the ratio of sample power to reactor power used previously.[15] The values used were subject to two corrections: one, of -9%, was applied to obtain agreement between calculated and measured cladding surface temperatures found necessary from the preliminary transient tests and one correction for sample burnup was also made.[16]

Table XVII shows the experimental conditions used in exposing the four pins (preliminary transients data are now shown). The calculated

TABLE XVII. Irradiated Oxide Sample Condition in TREAT

Sample	Pin Reference No.	Estimated Burnup (a/o)	Sample Energy Input (J/g)	Calc Max Fuel Temp (°C)	Calc Fuel Surface Temp at Time of Max Fuel Temp (°C)
1	1	0.70	757	2131	1582
2	11	2.95	1141	2750[a]	2011-2220[a]
3	3	0.91	869	2464	1809
4	9	3.45	728	2045	1508

[a]Fuel at melting point for 0.4 sec.

[14]Schoeberle, D. F., Miller, L. B., and Heestand, J., ANL-6654.

[15]Dickerman, C. E., et al., ANL-6845 (1965).

[16]This correction is in good agreement with the decrease in power ratio resulting from the change in TREAT core loading used previously.[15] In the previous test, the viewing slot extended into the reactor only far enough to accommodate the transparent capsule assembly. In this test, the core loading was changed to allow the viewing slot to extend through the core and permit testing the fast-neutron-hodoscope meltdown-viewing device.

fuel-clad interface temperatures were based upon a thermal conductance value of 0.25 W/cm-°C, which was deduced from an analysis of the shapes of the curves of cladding surface temperatures versus time obtained from the preliminary transients tests. A nominal TREAT burst had a duration of 0.5 sec.

2. Meltdown Experiment with TREAT Mark-II Integral Sodium Loop

Analyses have been performed of the high-specific-energy-input meltdown experiment, performed with a 6% enriched EBR-II Mark-I pin in flowing sodium in a Mark-I TREAT integral sodium loop. The sample pin was contained inside a ring of six hollow cladding tubes which were contained in the loop. The pin was subjected to a transient initiated with 1.9% k_{ex}. The TREAT reactor attained a maximum power of 1250 MW, and was scrammed at 500 MW-sec integrated power. The axial power profile was shaped. Maximum sample fuel power density at the axial midplane was 76 kW/cc, and the integrated power density in the sample fuel at the midplane up to the time of maximum power was 13.2 kW sec/cc.

In the previous failure analysis on EBR-II Mark-I pins cooled in stagnant sodium, the dominant mechanisms inducing failure were dissolution of the cladding by eutectic formation (a U-Fe eutectic causing penetration within approximately 1 sec once clad temperatures reached 1100-1150°C) and hoop stresses caused by internal pressure. However, to describe realistically the phenomena associated with the same transient nuclear heating of these fuel pins in a flowing sodium environment, a more complete analysis is needed, since thermal stresses and gross fuel motion must be considered. Thus, a reasonably accurate accounting of the following four factors must be made:

(1) tangential tensile stress induced in the cladding by internal pressure;

(2) tangential tensile stress induced in the cladding by radial temperature gradients within the clad itself;

(3) formation of U-Fe eutectic due to chemical interaction of the fuel with the cladding (consideration must be given to both the total amount of eutectic locally formed as well as to local deterioration of the cladding);

(4) motion of the fuel itself up to the time of cladding failure, if failure occurs.

The failure analysis is thus incomplete in that it does not consider the problem of analytically describing fuel motion or of treating directly eutectic formation. Transient temperature calculations were performed using the ARGUS code,[14] and factors 1-3 above were calculated by the use of simple models:

a. Thermal-stress Calculations. The calculation of hoop stresses in the clad resulting from the radial temperature gradient was done by means of the formula

$$\sigma_{\theta\theta} = \alpha E \Delta T / 2(1 - \nu),$$

where

$\alpha = 10^{-5}/°C$, the coefficient of thermal expansion;

$E = 23 \times 10^6$ psi, the elastic modulus;

$\nu = 0.3$, Poisson's ratio.

The formula does not consider elastic deformation but, aside from this limitation, is judged to be appropriate to the problem. In reality, deformation and yielding by the cladding relieve these stresses; however, calculated values of stresses greatly in excess of the tensile strength can be an indication of failure, despite yielding.

b. Hoop Stress due to Internal Pressure. Once the internal pressure is specified, the tangential stress it induces in the cladding is determined by the relation

$$\sigma_{\theta\theta} = P_I \frac{\gamma}{\Delta\gamma},$$

where

P_I = internal pressure;

γ = inner radius of cladding;

$\Delta\gamma$ = cladding thickness.

The (maximum) internal pressure was assumed to be the sum of the pressure due to the sodium bond and of the argon gas which fills the upper end of the capsule. The contribution of the sodium was determined by defining it as the vapor pressure associated with the maximum calculated bond temperature at each time interval. The contribution of the argon was specified by the perfect gas law. The mass of argon present is known so both the argon temperature and volume must be determined.

The argon temperature was defined by assigning to the gas 10% of the space-averaged temperature rise across the top of the fuel pin at each time interval.[17] The available volume was determined by using space

[17]This arbitrary method can be replaced by a calculation of the heat flux into the gas from the top of the fuel, using axial temperature gradients. But it is not clear how to take into account sodium that is above the fuel.

averages of the transient temperatures calculated for the fuel, bond, and clad. By means of the appropriate thermal expansion coefficients, the volume of each component of the pin was specified at each time interval. The volume of the bond and restrainer rod and of the fuel was subtracted from the total internal volume, giving the volume of the argon.

c. Penetration of Cladding due to Eutectic Formation. From the data of Walter and Kelman[18] for the penetration rate of U-5 w/o fissium alloy through 10-mil Type 304 stainless steel, the total penetration of the cladding as a function of time can be calculated, excluding per se effects of the eutectic itself (its thermal properties and its effects on the geometry of the system).

The calculations indicated that thermal stress at the location of maximum cladding temperature equaled the tensile strength at 1.3 sec after initiation of the excursion. By 1.36 sec, calculated thermal stress was twice the tensile strength, but eutectic attack of the cladding was negligible. At 1.36 sec, the sodium flow was abruptly halted, coincident with a sharp pressure spike recorded by the inlet pressure transducer. Not until 1.42 sec did the calculated cladding stress due to internal pressure reach the tensile strength of the cladding. In addition, at 1.36 sec, the calculated cladding surface temperature was only 700°C (calculated maximum coolant temperature at that time was only 500°C). Thus, the analysis indicates that:

(1) The initial pressure pulse and flow reversal at 1.36 sec was due to failure of the pin due to thermal stress.

(2) The second and final pressure pulse and flow reversal at 1.59 sec was due to extreme coolant vaporization rates caused by the coolant returning to the failed section after approximately 150 ms, during which time the pin was essentially insulated and exposed by the peak power (which occurred at 1.4 sec).

d. Sample Inspection. Inspection of the sample remains shows the pin to have failed. All pins in the test section were cast into place by solidified fuel, which necessitated slitting the fuel-holder tube longitudinally along a diameter and opening it like a book. The components of the test section were so firmly cast together that it was difficult to open the pipe, even after slitting, and impossible to do so without disturbing the contents. The regions of damaged pins appeared to extend farther downstream from the center than upstream. Most of the fuel had been ejected from its cladding, but some was retained in the lower 6-cm portion. However, the retained fuel had a "spongy" structure. A sample was taken for metallographic analysis. None of the

[18] Walter, C., and Kelman, L., J. Nucl. Met., 6, 281 (1962).

cladding remains had the appearance of a pressure failure, although such could have been obliterated by melting. All dummy pins were severely melted in the area of failure, probably by the molten fuel, some of which was found to have alloyed with all of the pins. Most of the fuel was deposited on the inner wall of the fuel-holder tube. This region of fuel deposits extended from about 5 cm below the fuel center to approximately the top of the fuel.

There was no evidence of extreme pressure within the test section, as none of the dummy pins were flattened, and the fuel holder did not appear to be bulged. No visual evidence of attack of the fuel-holder wall by molten fuel was found, but a metallographic sample was taken from the region of maximum fuel deposit for study.

Detailed study of the loop proper showed that its integrity was not compromised by the experiment.

3. Materials Behavior, Equation of State, and Energy Transfer

a. Coolant (Water) Expulsion Studies. The digital computer program written to smooth and differentiate the height versus time data is in the process of debugging. This program will yield expulsion velocities and accelerations which will be used to calculate voiding rates and the fraction of thermal input energy converted to fluid kinetic energy. A rough calculation has shown that this energy conversion is very inefficient in the experimental system used. A typical percentage of the thermal energy converted to kinetic energy is about 0.5% for highly saturated water. This conversion percentage decreases as the liquid temperature decreases.

All experimental expulsion work with water has ceased, and emphasis is now being placed on data interpretation, analytical model building, and the fabrication of a sodium expulsion experiment.

b. Superheat Experiments. This experiment is designed to measure the degree of liquid superheat required to initiate nucleate boiling in sodium under various conditions simulating a reactor environment. Typical parameters will be systematically varied to determine their independent and combined effects upon the liquid superheat necessary to initiate nucleation. The parameters to be examined are: (a) pressure, (b) dissolved gas content, (c) heat flux, (d) surface characteristics, and (e) the pressure-temperature history of the system.

Assembly of the initial superheat experiment is nearly complete. The system instrumentation is presently being checked.

c. Sodium Expulsion Experiment. In this experiment, it is planned to investigate the mechanism of coolant expulsion in a simulated reactor

environment. Fabrication of some of the components to be used in this experiment are complete, and the building of some of the instrumentation is underway.

d. Critical-flow Studies. Calculations of the progression of accidents in sodium-cooled reactors reveal that critical flow may exist in the core, leading to detrimental effects such as voidage of the coolant channel, shock phenomena, and pressure buildup.

The construction of experiments to study critical flow of different fluids is continuing. The fabrication of the argon gas cleaning system, the boiler, and blowdown vessel for the sodium loop has been completed. Final assembly of the loop components has been initiated.

e. Primary Containment by Energy Absorption. The computer program has been revised to incorporate the reactor vessel into the system. The reactor vessel is considered as a membrane. The energy associated with the reactor vessel is found by the use of the work-energy principle. The mechanical properties of the reactor vessel under dynamic biaxial stress are obtained from the static tensile (uniaxial) properties and the von Mises yield criteria, assuming a linear strain-hardening law for the material. The static tensile properties are used because the dynamic tensile properties are not readily available. Research work on the reactor vessel material should be conducted for dynamic loading.

The reactor vessel, assumed made of Type 304 stainless steel, is considered as an effective energy-absorbing device until it has reached a limiting strain value of 15%. Preliminary computer results show that the reactor vessel will absorb 20-25% of the total energy prior to rupture. Rupture is assumed to take place instantaneously, and the reactor vessel is assumed to disintegrate. The use of the reactor vessel as an energy-absorbing device will lessen the effect of the destructive component on the concrete containment vessel.

Concurrently, the computer program has been revised to obtain all of the computer output on tape. This will allow the program to run for a longer period of time without exceeding the core capacity. The final corrections and adjustments have been made, and the final computer results will be obtained soon.

f. Transient Heat Transfer Studies. An experimental study of the transient heat transfer from small hot particles moving through a liquid coolant is continuing. Knowledge of the rate and quantity of energy transfer that occurs between the fuel particles and the coolant is necessary in order to analyze the consequences of a reactor incident in which hot fuel materials may be dispersed into a liquid coolant. This study was initiated because neither theoretical nor experimental information is available to allow calculation of the heat transfer which occurs when small particles at high temperatures are rapidly dispersed in either water or liquid sodium.

(i) Experimental Measurements. The experimental apparatus (see Progress Report for June 1965, ANL-7071, p. 64) consists of a swinging arm (or pendulum) with a knife blade attached to the arm. A small metal sphere is attached to a thermocouple at the end of the blade. (The attachment is made by welding the wires of the Pt/Pt-10% Rh thermocouple to opposite sides of the sphere.) The metal sphere is heated in an electrical furnace to the desired temperature with the arm in a raised position. The raised arm is then released and, as it swings, the sphere is dragged through a tank of water or liquid sodium appropriately placed below the pivot of the arm. The time required for the ball to pass through the water or sodium is measured with an electronic counter-timer that is initiated and stopped by the impulses from two photocells. The photocells are triggered by the passage of the arm when the sphere enters and leaves the liquid.

Several series of experiments have been performed with a $\frac{1}{4}$-in.-dia nickel sphere in water. The sphere was initially heated to temperatures ranging from 150 to 1000°C. Experiments were performed with water temperatures of 30, 60, and 94°C at atmospheric pressure. The distance of travel through the water was varied by changing the water depth in the tank; path lengths of from 12 to 25.5 in. were employed. The average speed of the ball varied between 12 and 13 ft/sec owing to slight differences in the initial position of the arm.

The millivolt-time record from the thermocouple output was displayed on a Brown pen recorder and was used to determine the temperature of the sphere, both as it entered and as it left the water. Plots of the amount of decrease in the sphere temperature as it passed through the water versus the initial sphere temperature as it entered the water are given in Figs. 13, 14, and 15 for the data collected in 30, 60, and 94°C water, respectively.

In Fig. 13, four sets of data obtained in 30°C water are plotted. Two sets were obtained with the same water level in the tank and, thus, with constant path length (25.5 in.) and immersion time. The other two sets were for path lengths of 19.5 and 12 in. For each path length, the temperature drop increased smoothly with increasing initial sphere temperature. Indication of possible peaks around 1000°C were noted; however, since the maximum initial temperature achieved was only 1030°C, the peaks were not clearly delineated. Experiments involving the longer path lengths resulted in greater temperature drops; a maximum temperature drop of 410°C was observed for a sphere initially at 1000°C with a 25.5-in. path length through the water.

In Fig. 14, five sets of data are plotted that were obtained in 60°C water with path lengths of 12.0, 19.5, and 25.5 in. For all three path lengths, a peak in the temperature drop occurred with initial sphere temperatures in the range from 600 to 700°C. The maximum temperature drop recorded was about 260°C.

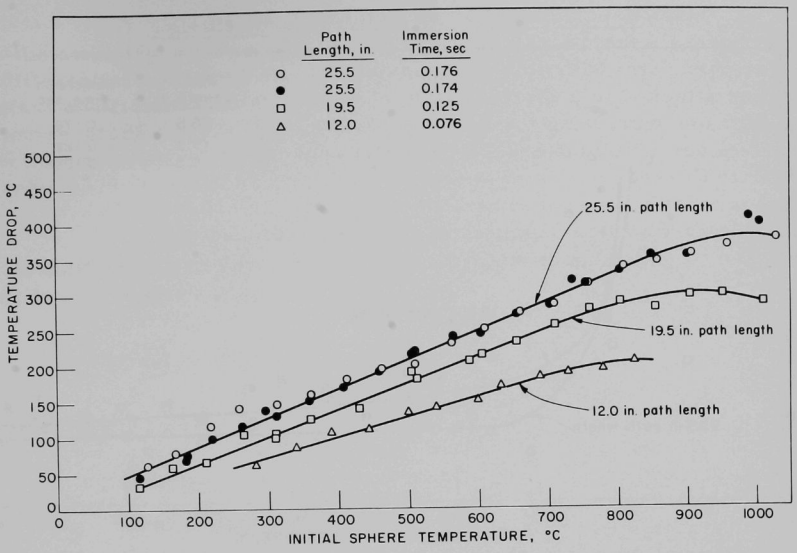

Fig. 13. Temperature Drop through 30°C Water as a Function of Initial Sphere Temperature for Swinging-arm Experiments (1/4-in. nickel sphere)

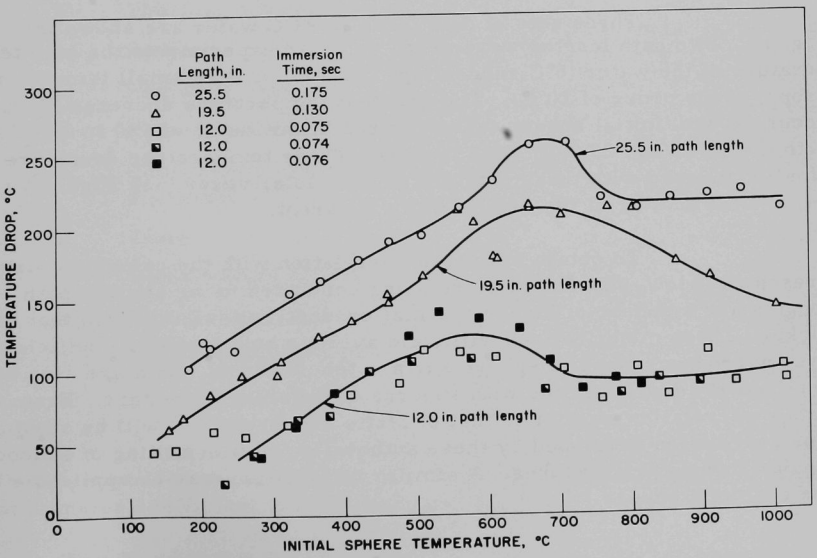

Fig. 14. Temperature Drop through 60°C Water as a Function of Initial Sphere Temperature for Swinging-arm Experiments (1/4-in. nickel sphere)

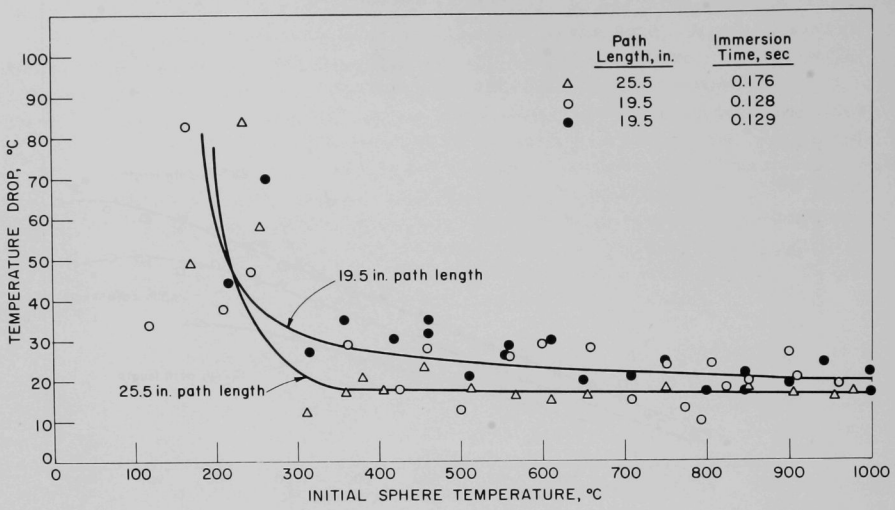

Fig. 15. Temperature Drop through 94°C Water as a Function of Initial Sphere Temperature for Swinging-arm Experiments (1/4-in. nickel sphere)

Three sets of data taken in 94°C water are shown in Fig. 15. Two path lengths were used. In these experiments the high temperature of the water (6°C subcooling) resulted in very small temperature drops (of the order of 20°C). The greatest temperature decrease (85°C) occurred with initial sphere temperatures in the range of 150 to 250°C for both the 19.5- and 25.5-in. path lengths. These temperature drops are very small compared with those obtained in the cooler water (see Figs. 13 and 14) and the scatter of the data is more apparent.

To obtain improved correlation with the calculated data presented below, experiments are being conducted using shorter path lengths and a sphere of higher thermal conductivity (silver) than that of nickel. These modifications will yield average heat transfer coefficients over narrower ranges of sphere surface temperature. Data are also being obtained at several speeds with spheres of different diameters. From these data a correlation similar to that of Motte and Bromley[19] will be attempted. The correlation developed by these authors is for film boiling of subcooled liquids flowing across tubes. A similar correlation may be applicable to the case of a sphere.

[19]Motte, E. I., and Bromley, L. A., Film Boiling of Flowing Subcooled Liquids, Ind. Eng. Chem. 49, 1921 (1957).

(ii) Calculational Studies. In order to evaluate the data taken with the swinging-arm apparatus, a computer program was written to solve the differential equations describing the energy flow in a sphere with a constant coefficient of heat transfer at the surface. The program calculates the temperature distribution and average surface heat transfer coefficient from the temperature drop, time of submersion, and physical properties of the sphere.

The program is based on the analytical solution of Carslaw and Jaeger[20] to the differential equation of heat conduction in a sphere derived from Fourier's law,

$$-k\frac{\partial}{\partial r}\left(r^2\frac{\partial T}{\partial r}\right) + r^2\rho C_p\frac{\partial T}{\partial t} = 0, \qquad (1)$$

where

ρ	Density
C_p	Heat capacity per unit mass
k	Thermal conductivity
h	Heat transfer coefficient
K	Thermal diffusivity ($= k/\rho C_p$)
r	Radius of shell
a	Radius of sphere
η	Nusselt number/2 ($= ha/k$)
α_n	Coefficients of the Carslaw and Jaeger solution (i.e., eigenvalues)
t	Time
T	Temperature at time t
T_1	Initial sphere temperature
T_W	Water temperature
n	Subscript integer.

Equation 1 assumes that the physical properties are constant with respect to temperature. The analytical solution, assuming a constant heat transfer coefficient and the boundary conditions

$$T = T_1 \text{ when } t = 0, \qquad (2)$$

[20] Carslaw, H. S., and Jaeger, J. C., Conduction of Heat in Solids, Oxford University Press (1959), p. 237.

$$\frac{\partial T}{\partial r} = 0 \text{ when } r = 0, \tag{3}$$

and

$$-k\frac{\partial T}{\partial r} = h(T - T_W) \text{ when } r = a, \tag{4}$$

has been shown to be

$$\theta = \frac{2\eta}{ar} \sum_{n=1}^{\infty} A_n \sin(\alpha_n r) \exp(-K\alpha_n^2 t), \tag{5}$$

where

$$A_n = \frac{\alpha_n^2 a^2 + (\eta - 1)^2}{\alpha_n^2[\alpha_n^2 a^2 + \eta(\eta - 1)]} \sin(\alpha_n a) \tag{6}$$

and

$$\theta = \frac{T - T_W}{T_1 - T_W}. \tag{7}$$

Values of α_n, where n = 1, 2, 3, ..., can be obtained as the roots of the equation

$$a\alpha_n \cot(a\alpha_n) + \eta - 1 = 0. \tag{8}$$

These equations were programmed for the CDC 3600 computer. Temperature-drop values at various initial sphere temperatures (see Figs. 13, 14, and 15), the corresponding immersion times, the weight and diameter of the sphere, and estimates of the physical properties in the temperature range of interest were inserted into the computer. The corresponding heat transfer coefficients calculated by the computer are plotted in Fig. 16 as a function of the average surface temperature[21] of the sphere for each of the three water temperatures.

Similarly, the average heat fluxes that were computed for each set of variables are plotted in Fig. 17, also as a function of the average surface temperature. A peak (maximum) flux occurs at 500°C for the 60°C water data and at about 800°C for the 30°C water data. For the 94°C water (6°C subcooling), the heat flux appears to be rising as the average surface temperature is lowered. The classic work of Nukiyama[22] suggests a

[21] The average of the measured temperature of the sphere as it enters the water and the computed surface temperature of the sphere as it leaves the water.

[22] Nukiyama, S., Maximum and Minimum Values of Heat Transmitted from Metal to Boiling Water under Atmospheric Pressure, J. Soc. Mech. Eng. Japan 37 (206), 367 (1934).

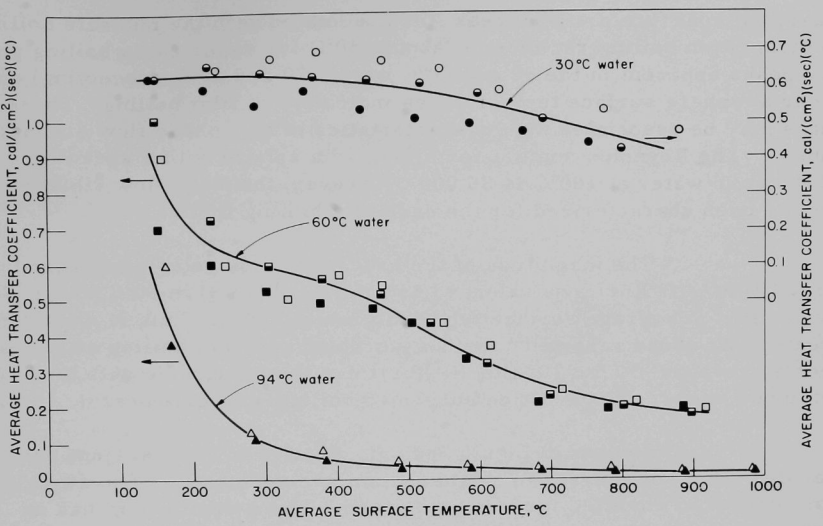

Fig. 16. Computed Heat Transfer Coefficients from Swinging-arm Experiments with 1/4-in.-dia Nickel Spheres (Speed of sphere through water = 12 ft/sec)

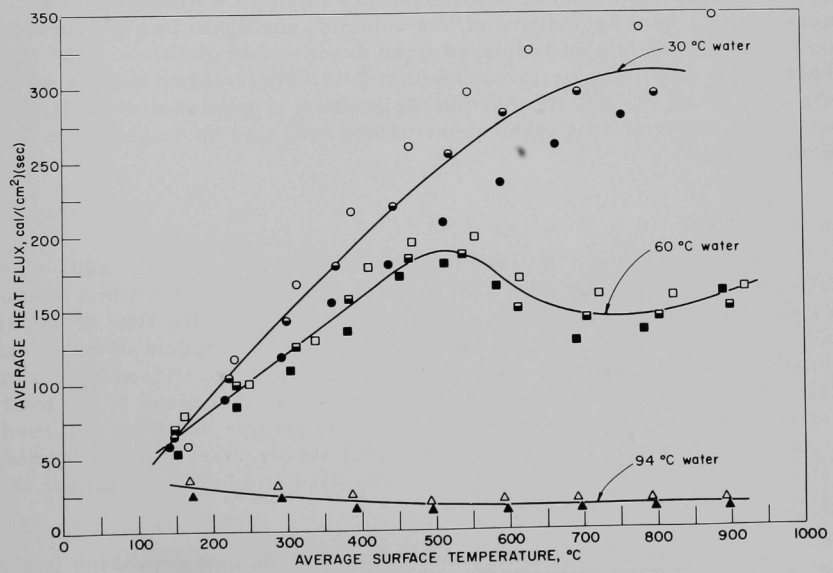

Fig. 17. Computed Heat Fluxes from Swinging-arm Experiments with 1/4-in.-dia Nickel Spheres (Speed of sphere through water = 12 ft/sec)

maximum heat flux, i.e., the peak flux associated with the nucleate boiling and transition boiling regimes, at about 150°C for water at its boiling point. The peaks apparent in the 30 and 60°C water (70 and 40°C subcooling) data occur at sphere surface temperatures indicative of film boiling. These peaks may be associated with characteristics of two-phase flow around the sphere. The Reynolds number for a $\frac{1}{4}$-in.-dia sphere with a speed of 12 ft/sec in water at 100°C is 80,000. However, the fluid-flow situation has not been characterized for the case of a boiling liquid.

The magnitude of the heat fluxes computed approached 4.6×10^6 Btu/(ft^2)(hr) [equivalent to 350 cal/(cm^2)(sec)] in 30°C water (70°C subcooling) at average surface temperatures of 800°C. This is considerably greater than those reported[22] for nonsubcooled nucleate boiling at atmospheric pressure [~0.5×10^6 Btu/(ft^2)(hr)], but is comparable with those fluxes obtained[19] in forced-convection subcooled boiling with cylinders.

(iii) Studies in Liquid Sodium. Studies of the transient heat transfer from hot spheres to liquid sodium are under way. The swinging-arm method in modified form is being used. The swinging arm has an 8-in. radius. Motion through the sodium is achieved using a printed-circuit d.c. motor of the type used to drive computer tape units. Remote operation of the motor has been achieved which allows the experimenter to move the sample sphere from a furnace through the sodium at a preset velocity, backward to a holding position at low velocity, and again into the furnace position. The equipment is housed in an argon-filled glovebox. The initial experiments are being performed with a $\frac{1}{2}$-in.-dia tantalum sphere equipped with a W-5% Re/W-26% Re thermocouple which is insulated with vitrified BeO. It is expected that other sphere sizes will also be employed in these studies.

4. TREAT

a. Operations. A metal-water reaction sample (CEN 220), consisting of three Zircaloy-clad UO_2 fuel rods, was irradiated while suspended in a stream environment above a pool of water. A flat-top type of transient was used to simulate more realistically some of the aspects of a loss-of-coolant incident. Data from thermocouples and pressure transducers indicate that prior to the sample falling into the water because of the melting, a metal-water reaction was in progress. The sample has been returned to Argonne, Illinois, for examination. Several steady-state runs were made to test some new neutron detectors and a modified amplifier circuit for the fast-neutron-hodoscope system.

b. Large TREAT Loop. Installation of the new expansion joints between the main system and the purification system was completed. Delivery of one additional expansion joint is scheduled for the first week in August. The loop will undergo a second 180-psig pressure test after this joint is installed to verify that the changes made following the first pressure test have corrected the deficiencies detected after the first test.

The finalized version of the design and safety analysis report was issued to members of the Reactor Safety Review Committee and the Idaho Division for review.

B. Effluent Control

1. Plutonium Volatility Safety

a. Chemistry of Tellurium Fluorides. Studies of the reactions of volatile tellurium fluorides are under way to determine the conditions whereby tellurium is fixed on solid materials and to investigate the kinetics of the reaction. Preliminary studies on the sorption of TeF_6 on Linde Molecular Sieve Type 13X (Runs 13X-1 through 13X-8) have been carried out at 25, 100, 200, 300, and 400°C. The sorbent has a nominal pore size of 10 Å and a surface area of 700 m^2/g. The results indicate that the capacity of the material for TeF_6 sorption decreases with an increase in temperature. Preliminary results indicate that Linde Molecular Sieve 13X is a good sorbent for TeF_6.

Similar experiments performed with soda lime as a sorbent indicated that this material is ineffective for sorbing TeF_6 over the temperature range from 25 to 300°C.

V. PUBLICATIONS

Papers

Measurement of Densities and Estimation of Critical Properties of the Alkali Metals
I. G. Dillon, P. A. Nelson, and B. S. Swanson
J. Chem. Phys. 44, 4229-4238 (June 1, 1966)

Outlook Brightens for Metallic Plutonium Fuels
J. H. Kittel
Nucleonics 24(7), 70-71 (July 1966)

Plutonium Management at Argonne National Laboratory
A. B. Shuck and J. H. Handwerk
Proc. Commercial Plutonium Fuels Conf., Washington, D.C., March 1-2, 1966. USAEC Report CONF-660308, p. 159-164

Thermoelastic Vibrations of a Thick Hollow Elastic Sphere
Gabriel Cinelli
J. Acoust. Soc. Am. 39(6), 1268 (July 1966) Abstract

Electron Multiplication Process in Proportional Counters
Raymond Gold and E. F. Bennett
Phys. Rev. 147, 201-213 (July 8, 1966)

ANL Reports

ANL-6950 A COST ESTIMATE FOR REMOTE REFABRICATION OF METALLIC FUELS
J. E. Ayer, D. A. Jones, D. D. Ebert, T. A. Buczwinski, and J. V. Sana

ANL-7143 REACTOR OSCILLATOR DETERMINATION OF CAPTURE-TO-FISSION RATIO IN AN UNDERMODERATED CRITICAL ASSEMBLY
W. C. Redman and M. M. Bretscher

ANL-7164 THE DEVELOPMENT AND FABRICATION OF A BORON ABSORPTION TUBE FOR SPECTROGRAPHIC ANALYSIS
J. T. Dusek

ANL-7165 TABLES FOR THE CALCULATION OF OPERATING PARAMETERS FOR SOLVENT-EXTRACTION COLUMNS
Terry R. Johnson and Nelda K. Clark